A molecular device for the redox quality control of GroEL/ES substrates

Emile Dupuy, Sander Egbert van der Verren, Jiusheng Lin, Mark Alan Wilson, Alix Vincent Dachsbeck, Felipe Viela, Emmanuelle Latour, Alexandra Gennaris, Didier Vertommen, Yves Frédéric Dufrêne, et al.

A molecular device for the redox quality control of GroEL/ES substrates

Emile Dupuy,[1,2,3] Sander Egbert Van der Verren,[3,4,5,] Jiusheng Lin,[6] Mark Alan Wilson,[6] Alix Vincent Dachsbeck,[1,2] Felipe Viela,[7] Emmanuelle Latour,[1,2] Alexandra Gennaris,[1,2] Didier Vertommen,[2] Yves Frédéric Dufrêne,[7] Bogdan Iuliu Iorga,[1,2,8] Camille Véronique Goemans,[1,2,9,*] Han Remaut,[4,5,*] Jean-François Collet[1,2,10*]

[1]WELBIO, Avenue Hippocrate 75, 1200 Brussels, Belgium

[2]de Duve Institute, Université catholique de Louvain, Avenue Hippocrate 75, 1200 Brussels, Belgium

[3]These authors contributed equally

[4]Structural Biology Brussels, Vrije Universiteit Brussel, 1050 Brussels, Belgium

[5]Structural and Molecular Microbiology, Structural Biology Research Center, VIB, 1050 Brussels, Belgium

[6]Department of Biochemistry and the Redox Biology Center, University of Nebraska, Lincoln, NE 68588, USA

[7]Louvain Institute of Biomolecular Science and Technology, Université Catholique de Louvain, Croix du Sud 4-5, 1348 Louvain-la-neuve, Belgium

[8]Université Paris-Saclay, CNRS UPR 2301, Institut de Chimie des Substances Naturelles, 91198 Gif-sur-Yvette, France

[9]European Molecular Biology Laboratory, Meyerhofstrasse 1, 69117 Heidelberg, Germany

[10] Lead contact

*Corresponding authors: Jean-François Collet (jfcollet@uclouvain.be), Camille Goemans (camille.goemans@embl.de), Han Remaut (han.remaut@vub.be)

SUMMARY

Hsp60 chaperonins and their Hsp10 cofactors assist protein folding in all living cells, constituting the paradigmatic example of molecular chaperones. Despite extensive investigations of their structure and mechanism, crucial questions regarding how these chaperonins promote folding remain unsolved. Here, we report that the bacterial Hsp60 chaperonin GroEL forms a stable, functionally relevant complex with the chaperedoxin CnoX, a protein combining a chaperone and a redox function. Binding of GroES (Hsp10 cofactor) to GroEL induces CnoX release. Cryo-electron microscopy provided crucial structural information on the GroEL-CnoX complex, showing that CnoX binds GroEL outside the substrate-binding site via a highly conserved C-terminal α-helix. Furthermore, we identified complexes in which CnoX, bound to GroEL, forms mixed disulfides with GroEL substrates, indicating that CnoX likely functions as a redox quality-control plugin for GroEL. Proteins sharing structural features with CnoX exist in eukaryotes, suggesting that Hsp60 molecular plugins have been conserved through evolution.

KEYWORDS:

Protein folding, chaperones, redox, proteostasis, TPR, thioredoxin, chaperonin

INTRODUCTION

Following synthesis as linear amino-acid chains, proteins must fold to unique three-dimensional (3D) structures to become functional. Seminal work from Anfinsen demonstrated that the information required for a polypeptide to reach its native conformation is contained in its primary sequence.[1] For most small proteins, folding to the native state is a spontaneous process that takes less than a few milliseconds.[2] For larger proteins with multiple domains, however, the path to the native conformation is more tortuous and potentially hazardous. For these proteins, stable intermediates can form, slowing the folding process and potentially leading to aggregation and/or degradation.[3] To deal with this problem, living cells express a network of chaperones that help complex proteins to fold efficiently.[4]

The Hsp60 chaperonins are a unique class of chaperones that are essential in all domains of life and prevent unproductive interactions within and between polypeptides using adenosine triphosphate (ATP)-regulated cycles.[5-7] Chaperonins stand out in the proteostasis network, as they form a complex tetradecameric structure encompassing a large cylindrical cage consisting of two seven-membered rings stacked back to back (**Figure S1A**).[8,9] Each Hsp60 subunit consists of an ATP-binding equatorial domain, an intermediate domain, and an apical substrate-binding domain (**Figure S1A**).[10] Hsp60 cooperates with Hsp10 [11], which forms a heptameric dome-like structure (**Figure S1A**).[12] In the presence of nucleotides, Hsp10 associates with the apical domain of Hsp60, binding as a lid covering the ends of the ring and forming a folding chamber[13] referred to as the "Anfinsen cage." Binding of Hsp10 to a substrate-loaded Hsp60 results in displacement of the substrate into the chamber, where it can fold protected from outside interactions.[14,15]

The mechanism by which chaperonins assist substrate proteins in navigating the folding landscape to their native state is relatively well understood. Although this is particularly true for the *Escherichia coli* Hsp60 chaperonin GroEL and GroES, its Hsp10 cofactor, several crucial questions remain unsolved. For instance, whether the GroEL-GroES nanomachine actively promotes folding or serves only as a passive folding cage remains controversial.[7] It is also unknown why some polypeptides are highly dependent on GroEL-GroES for folding whereas homologous proteins with a similar structure fold independently of the chaperonin.[7] Thus, further investigation is required to elucidate the sorting signals that recruit substrate proteins to the Hsp60 folding cage. Moreover, recent results have indicated that the integration of GroEL-GroES in the cellular proteostasis network also needs further exploration. Indeed, the identification of CnoX as the first chaperone capable of transferring its substrates to GroEL-GroES for active refolding[16,17] suggests that functional links between GroEL-GroES and accessory folding factors remain to be discovered. The extreme complexity of the GroEL-GroES molecular machine, its essential role in cell survival, and redundancy in the bacterial proteostasis system have slowed progress in the field, highlighting the need for new investigation approaches and experimental strategies.

Here, we sought to explore the details of the newly reported CnoX-GroEL functional relationship[16,17], with the aim of revealing unsuspected features of the GroEL-GroES system. CnoX consists of a redox-active N-terminal thioredoxin domain and a C-terminal tetratricopeptide (TPR) domain (**Figure S1B)**[18], a fold often involved in protein–protein interactions. CnoX is a "chaperedoxin," meaning that it combines a redox-protective function, by which it prevents irreversible oxidation of its substrates, and a holdase

chaperone activity, by which it maintains its substrates in a folding-competent state before transferring them to either GroEL-GroES or the DnaK-DnaJ-GrpE system for ATP-dependent refolding[16]. We reasoned that identifying the molecular attributes that uniquely allow CnoX to work in concert with GroEL-GroES would lead to new insights into the properties of the GroEL-GroES system.

RESULTS

CnoX and GroEL form a stable complex

To start our investigation, we pulled down CnoX from *E. coli* cellular extracts using specific α-CnoX antibodies. We found that CnoX co-eluted with only one partner (**Figure 1A**), a ~60-kDa protein identified as GroEL by mass spectrometry (MS), confirming previous results suggesting a direct interaction between the two proteins.[18] In this experiment, CnoX and GroEL were expressed from their native locus in cells grown under normal conditions. Noteworthy, intracellular protein abundance estimates[19] indicate that CnoX and GroEL tetradecamers ($GroEL_{14}$) are expressed at similar levels in rich defined medium at 37°C; thus, there seems to be enough CnoX to satisfy GroEL at a 1:1 CnoX:$GroEL_{14}$ ratio. Exposing the cells to heat shock (42°C) did not lead to an increase in the amount of GroEL that co-eluted with CnoX (**Figure S1C**).

We then examined whether the CnoX-GroEL interaction could be reconstituted *in vitro* using purified proteins. *E. coli* CnoX and GroEL were independently overexpressed and purified to near homogeneity (**Figure S1D**). We mixed GroEL and CnoX in a 1:1 molar ratio (1[GroEL subunit]:1[CnoX]) and found that they co-eluted from both a streptavidin affinity column (**Figure 1B**; a Strep-tag was fused to the N-terminus of CnoX) and a size-exclusion chromatography column (**Figure 1C**). The latter showed the co-eluting GroEL-CnoX complex in an approximately 14:1 molar ratio compared with the 1:1 input ratio, corresponding to a ratio of 1 CnoX per GroEL double ring. Notably, we also observed that CnoX formed a complex with a GroEL mutant ($GroEL_{R452A/E461A/S463A/V464A}$) known to form a single heptameric ring **(**$GroEL_7$; **Figure S1E)**.[20] Finally, we determined the affinity between the two proteins using fluorescence spectroscopy and fluorescence anisotropy and found that fluorescein

(fluorescein-5-maleimide [FM])-labeled CnoX (FM-CnoX) binds GroEL with a dissociation constant (K_d) of 310 ± 10 nM (**Figures 1D** and **S1F)**. Using atomic force microscopy (AFM), we measured a specific binding force of 175 ± 75 pN between the two proteins (**Figures S1G** and **S1H**)**.** Thus, we conclude that CnoX physically interacts with GroEL and that the two proteins form a stable complex both *in vitro* and *in vivo*.

GroES binding triggers the release of CnoX from GroEL

We next aimed to unravel the interrelationship among CnoX, GroEL, and GroES. GroES reversibly binds GroEL in the presence of nucleotides.[7,11] The addition of adenosine diphosphate (ADP), which triggers conformational changes in GroEL and primes the ring for GroES binding, had no impact on the GroEL-CnoX complex (purified proteins were mixed in a 14:1 molar ratio) (**Figure 1E**), although the affinity of CnoX for GroEL decreased slightly (K_d of ~350 nM) (**Figure S2A**). Strikingly, however, the subsequent addition of GroES (14[GroEL]:14[GroES]:1[CnoX] molar ratio) triggered the release of CnoX from GroEL (**Figure 1E**), indicating a direct or allosteric competition between CnoX and GroES for GroEL binding. We obtained similar results with a non-hydrolysable ATP analogue (**Figure S2B**). Next, titration of a complex between GroEL and FM-CnoX with increasing amounts of GroES resulted in a dose-dependent loss of FM-CnoX, confirming that GroES dissociates CnoX from GroEL (**Figure S2C**). Using a single-site competitive binding model, we calculated a fitted inhibitory constant (K_i) of 47 nM. Finally, under conditions in which GroES was overexpressed, the $GroEL_{R452A/E461A/S463A/V464A}$ variant ($GroEL_7$) did not co-elute with CnoX in pull-down experiments (**Figure S2D)**. Here, we employed $GroEL_7$ for unambiguous data interpretation. Altogether, these results clearly distinguish CnoX from typical GroEL substrates and indicate that CnoX is a *bona fide* GroEL partner. Indeed, GroEL does not

release substrate proteins such as unfolded citrate synthase (CS) upon GroES addition (**Figure 1E**); rather, these proteins become encapsulated inside the GroEL-GroES folding chamber for refolding.[6,7] Along the same line, we found that the presence of CnoX does not prevent GroEL from recruiting unfolded CS (**Figure S2E**). Thus, CnoX does not restrict access to the substrate-binding site of GroEL.

The C-terminal α-helix of CnoX binds GroEL near the site of substrate entry into the cage

Intrigued by these results, we sought to obtain structural information on the CnoX-GroEL interaction using cryo-electron microscopy (cryoEM). We reconstituted the CnoX-GroEL complex by mixing purified GroEL and $CnoX_{N\text{-}Strep}$ (10[GroEL]:1[CnoX] molar ratio, which corresponds to a ratio of 1[$GroEL_{14}$]:1.4 [CnoX]) in the absence of nucleotides. The complex was then affinity-purified (**Figure S3A**) and imaged for single-particle cryoEM analysis (**Figures S3B** and **S3C** and **Table S1**). Analysis of the two-dimensional (2D) class averages showed the two rings of GroEL stacked back-to-back and revealed the presence of a protruding density on top of the two GroEL rings (**Figures 2A, 2B,** and **S3D**). A c7-symmetrical 3D reconstruction resulted in a 3.4 Å electron potential map (**Figure S3E**) with a density on the GroEL apical domain corresponding to at least five α-helices and allowing an unambiguous rigid body docking with the TPR domain of CnoX (**Figures 2C, 2D, S3F,** and **S3G**). The absence of a clearly resolved thioredoxin domain in the CnoX-GroEL complex is consistent with the prior observation of extensive mobility of this domain in the X-ray crystal structure of CnoX alone.[18] This finding suggests that the thioredoxin domain is highly dynamic, which may be relevant for our proposed model (see below).

Although the N-terminal thioredoxin domain of CnoX is not visible, the structure provides crucial molecular details regarding the CnoX-GroEL interaction. First, the structure reveals that CnoX binds GroEL via its C-terminal α-helix (**Figure 3A, 3B, 3C)**; accordingly, a CnoX mutant lacking the last 10 C-terminal residues ($CnoX_{\Delta Cter}$) is unable to bind GroEL, both *in vivo* (**Figure 3D**) and *in vitro* (**Figure S4A).** Furthermore, addition of a His-tag to the C-terminus of CnoX ($CnoX_{C\text{-}His}$) or mutation of conserved residues in the C-terminal α-helix ($CnoX_{R277L}$, $CnoX_{Y284L}$) prevented CnoX binding to GroEL (**Figures 3D** and **S4A**). Using AFM, we found that the C-terminal α-helix on its own binds to GroEL; we measured a specific binding force of 135 ± 53 pN between GroEL and the 10 C-terminal residues of CnoX (**Figure S1I**), which is similar to the binding force measured between full-length CnoX and the chaperonin. We previously reported that CnoX is able to transfer unfolded CS to GroEL-GroES for refolding.[16] As shown in **Figure S4B**, we found that deleting the last 10 residues of CnoX significantly decreases its ability to cooperate with GroEL for CS refolding. Thus, the C-terminal α-helix of the TPR domain of CnoX functions as a specific GroEL affinity tag that is required and sufficient for GroEL binding and is important for function.

Using cells lacking trigger factor (Δ*tig*) and a functional DnaK-DnaJ-GrpE system (Δ*dnaKdnaJ*), we obtained further *in vivo* evidence that the C-terminal α-helix controls the CnoX-GroEL interaction. Δ*tig*Δ*dnaKdnaJ* cells exhibit a heat-sensitive phenotype that is rescued by overexpression of GroEL-GroES[21], presumably because the chaperonin, when present at high levels, folds proteins that normally depend on trigger factor and/or DnaK-DnaJ-GrpE. We found that overexpressing CnoX, but not $CnoX_{\Delta Cter}$, together with GroEL-GroES prevents the chaperonin from suppressing the growth defect of Δ*tig*Δ*dnaKdnaJ* cells at 37°C (**Figure S4C**). This result suggests that CnoX, when bound to GroEL, limits the ability of the chaperonin to

fold non-substrate proteins. This finding further demonstrates the importance of the C-terminal α-helix and provides additional evidence that the GroEL-CnoX interaction occurs *in vivo*. Finally, we noted that while the sequence of the TPR domain of CnoX is diverse among species, the last C-terminal helix is highly conserved (**Figure S4D**) and is structurally and electrostatically distinct from the remainder of the TPR domain[18], suggesting that the ability to bind GroEL is widespread and central to CnoX activity.

The structure also reveals where CnoX binds to GroEL; the interaction zone, which has a buried surface area of 472 Å^2 (-4.6 kcal/mol; PDBePISA[22]) and encompasses residues D224, K286–M307, K311, D316, R345, and Q348 (**Figures 3B** and **3C**), corresponds to a shallow surface cleft formed by helices J and K in the apical domain of GroEL. This region does not overlap with the substrate-binding site of GroEL in helices H and I[6,7], as also corroborated by the above results (**Figure S2E**). At least five potential hydrogen bonds or electrostatic interactions stabilize the contacts between CnoX and GroEL (R255-E304, R277-G298, R277-T299, Y284-E304, and Y284-R345, listed as CnoX-GroEL), as well as a hydrophobic interaction between CnoX residues L279, Y280, and L283 and GroEL residues V300, I305, and M307 (**Figures 3B** and **3C**). Accordingly, introducing a set of mutations in the interaction interface of GroEL (GroEL§) with CnoX disrupted the GroEL-CnoX interaction (**Figure 3E)**, without affecting the chaperone function of GroEL as the mutant was still able to rescue the temperature sensitivity of Δ*tig*Δ*dnaKdnaJ* cells (**Figure S4C**).

GroEL is a highly dynamic protein that undergoes substantial conformational rearrangements depending on the binding of a nucleotide, its position in the folding pathway, or the binding of GroES[23]. Comparison of our structure with the different

conformational states of GroEL shows that the GroEL rings are in a conformation corresponding to that of the nucleotide-free protein (**Figure S4E**), as expected. Our findings also indicate that the CnoX-binding paratope remains fully accessible in all conformations, except when GroES is bound (**Figure S4E**). The persistence of the CnoX-binding site in various conformations of GroEL is consistent with the ability of CnoX to bind to GroEL irrespective of the presence of a nucleotide (**Figures 1B, 1C, 1E,** and **S2B**). Available structures also show a large conformational rotation of the GroEL apical domain in the GroEL-GroES complex. Although the GroES-binding site does not directly overlap with that of CnoX, the conformation of the apical domain results in a steric occlusion of the CnoX-binding paratope (**Figure S4E)**, providing a molecular explanation to our finding that GroES docking onto GroEL is incompatible with CnoX binding (**Figures 1E** and **S2B**).

CnoX forms mixed disulfides with obligate GroEL substrates when bound to GroEL

We next aimed to gain insight into the physiological relevance of the CnoX-GroEL complex *in vivo*. GroEL-GroES substrates often need minutes to fold after leaving the ribosome[24], which raises a question regarding how their amino acids are protected from oxidative damage before reaching their native state. This question is particularly relevant for cysteine residues, which are highly sensitive to oxidation by the molecular oxidants present in cells even in the absence of stress.[25,26] Indeed, the thiol side chain of a cysteine is readily oxidized to a sulfenic acid (-SOH), an unstable derivative that can react with another cysteine in the vicinity to form a disulfide or that can be irreversibly oxidized to sulfinic and sulfonic acids. Similar to Anfinsen's experiments showing that noncanonical disulfide pairing thwarts *in vitro* protein folding, one can expect the GroEL chaperonin to require its substrates' cysteines to be reduced for proper folding. CnoX stands out in the proteostasis network in

239 that it combines a chaperone and a redox-protective function;[16] therefore, CnoX may bind
240 GroEL to function as a redox rescue mechanism for slow-folding GroEL-GroES substrates.
241
242 By performing additional pull-down experiments, we obtained a crucial result shedding light
243 onto the function of CnoX. When GroEL is pulled down from cellular extracts, it co-elutes
244 with CnoX, as expected. Intriguingly, we found that high-molecular-weight complexes
245 involving CnoX are also pulled down (**Figure 4A**). When a reducing agent was added, these
246 complexes disappeared, indicating that they correspond to mixed disulfides comprising CnoX
247 and unknown proteins. Accordingly, we did not detect high-molecular-weight complexes
248 when the experiment was repeated with a CnoX mutant lacking the two cysteine residues
249 ($CnoX_{no\_cys}$; **Figure 4A**), confirming that tripartite complexes of GroEL, CnoX, and unidentified
250 proteins exist in the cell. We identified the proteins involved in the mixed disulfides using MS
251 (**Table S2**); remarkably, the identified proteins exhibited strong enrichment in GroEL obligate
252 substrates (9 of the 57 obligate GroEL substrates were detected[27]), including two low-
253 abundance proteins, acetylornithine deacetylase, and nicotinamide adenine dinucleotide
254 phosphate (NADP)-specific glutamate dehydrogenase (<400 copies per cell;[19]) (**Figure 4B** and
255 **Table S2**). We did not detect these proteins when the experiment was performed using
256 lysates prepared from cells expressing $CnoX_{no\ cys}$. Thus, we conclude that CnoX forms mixed
257 disulfides with obligate GroEL substrates when bound to GroEL in the cell.
258
259 **CnoX functions as a molecular plugin providing redox quality-control for GroEL substrates**
260 Altogether, our results suggest the following model (**Figure 4C**). Regardless of stress, CnoX
261 binds GroEL via its highly conserved C-terminal α-helix in a nucleotide-independent manner.
262 The CnoX-binding interface on GroEL does not overlap with the substrate-binding site. If the

substrate that reaches GroEL for folding presents oxidized cysteine residues (to a sulfenic acid or in a disulfide bond), CnoX reacts with the substrate via the cysteines of its thioredoxin domain, resulting in the formation of a mixed disulfide. Cytoplasmic reducing pathways then reduce the mixed disulfide, releasing the substrate in a reduced, folding-competent state. The binding of GroES to GroEL induces conformational changes in the chaperonin and occludes the CnoX-binding site, triggering CnoX release from GroEL and encapsulation of the substrate within the folding cage for folding.

This model implies that segments of unfolded substrates are already present in the cavity of GroEL when the substrates form a mixed disulfide with GroEL-bound CnoX. We confirmed this implication by purifying a tripartite complex of $CnoX_{N\text{-}Strep}$, CS, and GroEL (**Figure 5A**) and subjecting it to crosslinking MS analysis: we detected crosslinked peptides between several GroEL residues, including four facing the inside of the cavity, and CS (**Figures 5B** and **5C**). Thus, we propose that CnoX functions as a molecular plugin that provides redox quality control for GroEL substrates. Our model is compatible with both the binding of CnoX to unfolded oxidized client proteins in solution followed by delivery to the GroEL chaperonin and the surveillance performed by CnoX to identify erroneously oxidized client proteins that may become stuck at the substrate entrance to the Anfinsen cage of GroEL. This function of CnoX as a quality control plugin for GroEL is constitutive and not inducible by stress. It is not incompatible with the previously reported role of CnoX in the protection of cellular proteins, including GroEL substrates, from HOCl-induced aggregation and oxidation.[16]

DISCUSSION

Investigations of Hsp60 chaperonins started in the 1970s[6], when researchers described mutations that blocked phage head assembly in *groE* and discovered the tetradecameric structure of GroEL, the archetypical member of the Hsp60 family, using EM. Since then, a large body of studies has examined the mechanistic and structural properties of Hsp60 proteins and their Hsp10 co-chaperones, not only in bacteria but also in chloroplasts and mitochondria.[6] This impressive amount of work has rendered chaperonins a textbook example of folding systems. In the current study, the identification of CnoX as a quality-control protein that physically interacts with GroEL-GroES for optimal folding has further widened this field of investigation by uncovering an unsuspected feature of Hsp60. Additional questions remain unsolved and will be the subject of future research. For instance, the biologically active stoichiometry of the CnoX-GroEL complex warrants careful investigation, as well as the specific role of the cytoplasmic reducing pathways in the reduction and release of mixed disulfides. Future work must also establish the location of the N-terminal thioredoxin domain when CnoX is bound to GroEL. Our results show that CnoX forms mixed disulfides with GroEL substrates while being bound to GroEL, but future research will elucidate whether CnoX also functions as a tugboat to locate endangered GroEL substrates in the cytoplasm and escort them to the chaperonin. Finally, it will be important to determine whether similar proteins with a redox quality-control function exist in other organisms, including eukaryotes. The facts that *E. coli* CnoX stably interacts with human mitochondrial Hsp60 (mHsp60; **Figure S5A**) and that proteins sharing structural features with CnoX exist in eukaryotes (**Figures S5B, S5C,** and **S5D**) support this idea. Along the same line, it is tempting to speculate that living cells could also contain Hsp60 molecular "plugins" with specific, redox-independent functions yet to be discovered.

Limitations of the study

Our study focused on the interaction between CnoX and GroEL. We did not study the ability of CnoX to cooperate with the DnaK-DnaJ-GrpE system. Moreover, although we identified several eukaryotic proteins with structural features similar to those of CnoX —which suggest that these proteins could function as molecular plugins for eukaryotic Hsp60 proteins— we did not investigate this attractive hypothesis. Our model implies that cytoplasmic reducing systems catalyze the reduction of mixed disulfides between CnoX and its substrates. The respective roles of the thioredoxin and glutaredoxin pathways in this process remain to be determined. Further studies are also required to obtain additional structural information on the ternary complexes between GroEL, CnoX, and their substrates.

STAR METHODS

Detailed methods are provided in the online version of this paper and include the following:

- Key resources table
- Resource availability
    - Lead contact
    - Materials availability
    - Data availability
- Method details
- Quantification and statistical analysis

SUPPLEMENTAL INFORMATION

Table S2: Proteins involved in the mixed disulfides with CnoX, related to Figure 4.

Proteins were pulled down with the GroEL-CnoX complexes using a-GroEL antibodies and identified using LC-MS/MS. These proteins were not detected when the experiments were repeated in cells expressing $CnoX_{no\_cys}$.

ACKNOWLEDGEMENTS

We thank Asma Boujtat and Gaetan Herinckx for technical help. We are indebted to Dr. Michael Deghelt, Dr. Seung-Hyun Cho, and Dr. Pauline Leverrier for helpful suggestions and discussions and for providing comments on the manuscript. M.A.W. received support from National Institutes of Health grant R01GM139978. We thank Dr. Tommi White and Dr. Javier Seravalli for assistance with the GroEL-CnoX quantitative interaction studies and Dr. Aron Fenton for discussions about cooperative protein binding. We thank the staff at the VIB-VUB facility for Bio Electron Cryogenic Microscopy (BECM) for assistance in data collection. This work was funded by the Fonds de la Recherche Scientifique (FNRS) grant agreements WELBIO-CR-2015A-03 and WELBIO-CR-2019C-03, the Excellence of Science in Research Program of the FWO and FRS-FNRS (G0G0818N), the Fédération Wallonie-Bruxelles (ARC 17/22-087), GENCI-IDRIS (2021-A0100711524), the Flanders Research Foundation Hercules grant (G0H5916N), the Flanders Research Foundation PhD fellowship program, and the Flanders Institute for Biotechnology – VIB.

AUTHOR CONTRIBUTIONS

Writing: JFC, SEVdV, ED, HR, and CVG. Conceptualization: CVG, ED, HR, and JFC. Investigation, strain construction, construct cloning: ED, CVG, AVD, AG, SEVdV, JL, MAW, EL, YFD, and FV. Identification and AlphaFold modeling of CnoX mammalian homologs: BII. Mass

spectrometry: DV. Data analysis and interpretation: ED, SEVdV, CVG, HR, JL, MAW, YFD, FV, and JFC. All authors discussed the results and commented on the manuscript.

DECLARATION OF INTERESTS

The authors declare no competing interests.

Main Figure Titles and Legends

Figure 1. CnoX interacts stably with GroEL.

(A) GroEL co-elutes with CnoX when CnoX is pulled down from wild-type cell extracts using α-CnoX antibodies. Both proteins are absent when the experiment is repeated with extracts prepared from the Δ*cnoX* mutant. The image of sodium dodecyl sulphate–polyacrylamide gel electrophoresis (SDS-PAGE), stained with Coomassie blue, is representative of >3 replicates. * indicates the light and heavy chains of the antibodies.

(B) Purified $CnoX_{N\text{-}Strep}$ and GroEL form a complex that can be isolated using streptavidin affinity purification. Two fractions are shown.

(C) Purified CnoX and GroEL form a complex that can be isolated using size-exclusion chromatography.

(D) Formation of a complex between FM-CnoX and GroEL can be monitored using fluorescence anisotropy. The noncooperative model gives an adequate fit to these data, with a K_d of 310 ± 10 nM.

(E) CnoX and unfolded CS co-elute with GroEL from a gel filtration column. Addition of GroES triggers the release of CnoX from GroEL, while CS remains bound to GroEL. Size-exclusion chromatography was performed in the presence of ADP (50 μM), and fractions were analyzed by SDS-PAGE. The results are representative of >3 experiments.

Figure 2. CryoEM shows that the TPR domain of CnoX binds GroEL.

(A, B) CryoEM 2D class averages of the GroEL-CnoX complex reconstituted *in vitro* at a 10:1 molar ratio (scale bar: 100 Å).

(C, D) Side and top view of the structure of the GroEL-CnoX complex shown as a solvent-accessible surface. The equatorial, intermediate, and apical domains of GroEL are shown in slate, orange, and light cyan, respectively, and CnoX is shown in pink.

Figure 3. The C-terminal α-helix of CnoX binds a shallow cleft in the apical domain of GroEL.

(A) Ribbon representation of a single GroEL-CnoX protomer. CnoX binds GroEL via its C-terminal α-helix. The intermediate and apical domains of GroEL are shown in orange and light cyan, respectively. CnoX is shown in pink. For comparison, the GroEL-CnoX structure is shown superimposed on the structure of T-state GroEL (yellow; Protein Data Bank [PDB]: 1GRL).

(B, C) Close-up views of the GroEL-CnoX binding interface. CnoX binds GroEL through the following hydrogen-bond and electrostatic interactions (CnoX-GroEL): R255-E304, R277-G298, R277-T299, Y284-E304, and Y284 C-term-R345. For comparison, the GroEL-CnoX structure is shown superimposed on the structure of T-state GroEL (yellow; PDB: 1GRL).

(D) GroEL co-elutes with CnoX (lane 1) but not with $CnoX_{\Delta Cter}$ (lane 2), $CnoX_{R277L}$ (lane 3), $CnoX_{Y284L}$ (lane 4), or $CnoX_{C\text{-}His}$ (lane 5) when CnoX is pulled down from cell extracts using α-CnoX antibodies. In these experiments, CnoX and its variants were expressed in Δ*cnoX* cells. The SDS-PAGE gel, stained with Coomassie blue, is representative of >3 replicates.
* indicates the light and heavy chains of the antibodies.

(E) $GroEL^{\S}$, a GroEL variant with mutations in the CnoX-binding site (G298A/T299L/V300K/E304L/I305K/M307K/R345L), does not elute together with CnoX from a size-exclusion chromatography column (right), in contrast to wild-type GroEL (left). Three consecutive elution fractions are shown for each chromatography column.

Figure 4. CnoX functions as a molecular plugin to rescue GroEL substrates from oxidative damage.

(A) CnoX co-elutes with GroEL when the chaperonin is pulled down from wild-type cell extracts using specific antibodies. High-molecular-weight complexes corresponding to dithiothreitol (DTT)-sensitive mixed disulfides are detected by α-CnoX antibodies. These complexes are not detected when the experiment is repeated using extracts from cells expressing a CnoX mutant lacking the two cysteine residues, $CnoX_{no\_cys}$.

(B) Obligate GroEL substrates trapped in mixed-disulfide complexes with CnoX and pulled down using α-GroEL antibodies were identified by liquid chromatography with tandem MS (LC-MS/MS).

(C) Model: 1. CnoX forms a stable complex with GroEL via its C-terminal α-helix in a nucleotide-independent manner. Positioned on the apical domain of GroEL, CnoX interacts with incoming substrates for GroEL, acting as a redox quality-control plugin. 2. If the substrate that reaches GroEL for folding presents oxidized cysteine residues (to a sulfenic acid or in a disulfide bond), CnoX reacts with the substrate via the cysteines of its thioredoxin domain, and a mixed disulfide is formed. Interactions between the substrate and the GroEL cavity occur. 3. Cytoplasmic reducing pathways reduce the mixed disulfide, releasing the substrate in a reduced, folding-competent state. 4. GroES binding triggers CnoX release from GroEL and encapsulation of the substrate within the folding cage for folding.

Figure 5. Unfolded CS is present in the cavity of GroEL when in a mixed disulfide with CnoX.

(A) Co-overexpression of $CnoX_{N\text{-}Strep}$, CS, and GroEL leads to the formation of a ternary complex that was purified by affinity chromatography (left) and size-exclusion chromatography (right).

(B) The ternary complex was treated with disuccinimidyl sulfoxide (DSSO) —a crosslinker with an amine-reactive N-hydroxysuccinimide ester at each end of a 7-carbon spacer arm— and subjected to proteolytic digestion with trypsin. The resulting peptide mixture was analyzed by LC-MS/MS. Seven crosslinked peptides between GroEL residues and CS were detected.

(C) Four of the GroEL residues that crosslink to CS face the inside of the cavity.

Supplemental Figure Titles and Legends

Figure S1. Molecular dissection of the interaction between the CnoX chaperedoxin and the GroEL-GroES nanomachine, related to Figure 1

(A) Structure of the GroEL-GroES complex from *E. coli* (PDB: 1AON). The apical, intermediate, and equatorial domains of GroEL are shown in light cyan, orange, and slate, respectively. GroES is shown in deep purple.

(B) Structure of *E. coli* CnoX (PDB: 3QOU).[18] The N-terminal thioredoxin domain, with its two cysteine residues, is shown in orange. The C-terminal TPR domain is shown in gold. The last C-terminal residues are shown in purple.

(C) The amount of GroEL that co-elutes with CnoX does not increase when CnoX is pulled down from extracts prepared from cells exposed to 42°C for 1 h instead of 37°C. We pulled down CnoX using α-CnoX antibodies. The SDS-PAGE gel, stained with Coomassie blue, is representative of >3 replicates. * indicates the light and heavy chains of the antibodies.

(D) GroEL and CnoX were purified to near homogeneity.

(E) $GroEL_{R452A/E461A/S463A/V464A}$, a GroEL variant that forms a single ring ($GroEL_7$), co-elutes with CnoX from a size-exclusion chromatography column.

(F) Binding of FM-CnoX to GroEL was monitored via the fluorescence emission intensity of the fluorescein label on FM-CnoX. We performed measurements in triplicate, with the standard deviations indicated. The dotted line indicates the best fit for the noncooperative model, and the solid line presents a fitted curve for the positively cooperative model, with K_d = 227 nM and Hill coefficient (nH) = 1.9.

(G) Schematic representation of the AFM setup for single-molecule force spectroscopy experiments: GroEL is attached to a gold-coated glass coverslip via a D490C substitution, and CnoX is attached to the cantilever via an N-terminal cysteine-containing linker.
(H) AFM measurement of the specific adhesion force between CnoX and GroEL. Two typical adhesion force curves are shown in the inset. We measured a specific binding force of 175 ± 75 pN (mean and standard deviation for a total of 5000 curves from three independent experiments). In these experiments, we used a GroEL mutant ($GroEL_{D490C}$) with a cysteine residue exposed on its equatorial domain to allow binding to the gold surface and a CnoX variant ($CnoX_{N\text{-}link/C38A/C63A}$) lacking the two cysteines of the thioredoxin domain to prevent disulfide bond formation between CnoX and GroEL.
(I) AFM measurement of the specific adhesion force between the C-terminal 10 residues of CnoX and GroEL. We measured a specific binding force of 135 ± 53 pN (mean and standard deviation for a total of 5000 curves from three independent experiments). In these experiments, we used a GroEL mutant ($GroEL_{D490C}$) with a cysteine residue exposed on its equatorial domain to allow binding to the gold surface.

Figure S2. GroES binding to GroEL displaces CnoX from the chaperonin. CnoX binding to GroEL does not prevent GroEL from recruiting substrates, related to Figure 1

(A) Nucleotide binding to GroEL decreases the affinity for CnoX. We monitored the binding of FM-CnoX to GroEL in the presence of ADP using the fluorescence emission intensity of the fluorescein label on FM-CnoX. Dotted lines indicate best-fit curves for the noncooperative model, and solid lines present best-fit curves for the positively cooperative binding model. ADP occupancy on GroEL reduces the binding affinity of FM-CnoX to 350 nM. Error bars

represent standard deviations from the results of three or more independent measurements.

(B) CnoX and unfolded CS co-elute with GroEL from a gel filtration column. The addition of GroES triggers the release of CnoX from GroEL, while CS remains bound to GroEL. We performed size-exclusion chromatography in the presence of 50 μM adenylyl-imidodiphosphate (AMP-PNP), a non-hydrolysable ATP analogue, and analyzed fractions by SDS-PAGE. The results are representative of >3 experiments.

(C) GroES displaces bound CnoX from GroEL. We added GroES to preformed FM-CnoX:GroEL in the absence (brown) and presence (black) of ATP and monitored the fluorescence intensity of FM-CnoX. The addition of GroES causes FM-CnoX:GroEL to dissociate with a K_i of 47 nM only when ATP is present. Error bars represent standard deviations from the results of three or more independent measurements.

(D) $GroEL_{R452A/E461A/S463A/V464A}$ ($GroEL_7$) co-elutes with CnoX (lane 1) when CnoX is pulled down from cellular extract of cells overexpressing this GroEL single-ring variant. When GroES is co-overexpressed, $GroEL_7$ does not co-elute with CnoX, indicating that GroES displaces CnoX from GroEL *in vivo* (lane 2). * indicates the light and heavy chains of the antibodies.

(E) The GroEL-CnoX complex was incubated with or without unfolded CS. We pulled down GroEL using specific α-GroEL antibodies. Both CnoX and unfolded CS coimmunoprecipitated with GroEL, indicating that CnoX binding does not prevent GroEL from recruiting unfolded CS. * indicates the light and heavy chains of the antibodies.

Figure S3. Single-particle cryoEM analysis of the purified GroEL-CnoX complex, related to Figure 2

(A) Affinity purification of GroEL-CnoX (10[GroEL]:1[CnoX] molar ratio, which corresponds to a ratio of 1[$GroEL_{14}$]:1.4 [CnoX]). * indicates the fraction used for grid preparation.
(B) Representative cryoEM micrographs in thin (left) and thick (right) ice, displaying predominately side (i), top (ii), and tilted (iii) views (scale bar: 100 nm; i, ii, iii labeled as in Figure 2B).
(C) Single-particle cryoEM processing pipeline. We optimized 3D map representations for CnoX density.
(D) Reconstructed 3D electron potential map showing a good density for GroEL and sparse density for CnoX spokes.
(E) FSC model map, as generated by Phenix.
(F) Density-fit illustrations of the GroEL-CnoX structure. The final 3D reconstruction is displayed as density-modified (surface) and locally sharpened (mesh) maps, which were best-suited for building GroEL and CnoX, respectively. The 3D reconstructions present a close-up view of the GroEL-CnoX contact region (top left and right, 90° rotated), a close-up view of the GroEL equatorial region (lower left), and a global particle view (lower right). Individual GroEL (purple) and CnoX (pink) subunits are highlighted for clarity.
(G) Side view of the GroEL-CnoX structure as resolved and built into the 3D cryoEM reconstruction (shown in surface representation) and the relative positioning of the CnoX thioredoxin domain (ribbon representation) based on a superimposition of the X-ray structure of *E. coli* CnoX (PDB: 3QOU) onto the CnoX TPR domain resolved in the 3D cryoEM reconstruction.

Figure S4. CnoX binds GroEL via its conserved C-terminus, related to Figure 3

(A) GroEL was mixed with CnoX, $CnoX_{\Delta Cter}$, or $CnoX_{C\text{-}His}$, and specific α-CnoX or α-GroEL antibodies were used to pull down the corresponding protein. We observed an interaction between CnoX and GroEL only for wild-type CnoX, not for $CnoX_{\Delta C\text{-}ter}$ or $CnoX_{C\text{-}His}$, indicating that CnoX binds GroEL via its C-terminus. The SDS-PAGE gel, stained with Coomassie blue, is representative of >3 replicates. * indicates the light and heavy chains of the antibodies. **(B)** CS, chemically unfolded with guanidine hydrochloride, was diluted in a buffer containing various combinations of CnoX (6:1 ratio to CS), $CnoX_{\Delta Cter}$ (6:1 ratio to CS), GroEL-GroES, and ATP. Here, the recovered activity of CS serves as a proxy to quantify CS refolding. These results demonstrate that deleting the C-terminal α-helix of CnoX decreases the ability of CnoX to transfer CS to GroEL-GroES for refolding. This graph shows the mean of three independent experiments; error bars represent the standard error of the mean. Differences were evaluated with Student's t-test ($p > 0.05$, $^{**}p < 0.01$, $^{***}p < 0.001$, $^{****}p < 0.0001$). **(C)** Overexpression of GroEL-GroES (from the p29SEN plasmid) rescues the temperature sensitivity of Δ*tig*Δ*dnaKdnaJ* cells. Co-overexpression of CnoX prevents this rescue, unless the C-terminal α-helix ($CnoX_{\Delta Cter}$) is deleted. Introducing mutations in the CnoX-binding site in GroEL ($GroEL^{\S}$—G298A/T299L/V300K/E304L/I305K/M307K/R345L) does not alter the ability of GroEL to rescue the temperature sensitivity of Δ*tig*Δ*dnaKdnaJ.* **(D)** Sequence logo showing the high conservation of the 10 C-terminal residues of CnoX among *E. coli, Shigella flexneri, Klebsiella pneumoniae, Enterobacter ludwigii, Serratia plymuthica, Pseudomonas fluorescens, Pantoea ananatis, Stenotrophomonas sp. DAIF1, Citrobacter freundii, Erwinia sp. Ejp617, Halomonas sp. HL-93, Cronobacter turicensis, Marinobacter sp. BSs20148, Salmonella enterica, Pseudomonas aeruginosa, Yersinia enterocolitica, Burkholderia gladioli,* and *Stenotrophomonas maltophilia* (https://weblogo.berkeley.edu/).

552

553 **(E)** The different conformational states of the GroEL apical domain are compatible with CnoX
554 binding, except in the GroEL-GroES complex. Side-view surface representation of the cryoEM
555 structure of GroEL-CnoX (left), side by side with structures of GroEL in different
556 conformational states: the apo or T state (PDB: 1grl; [10]), the Rs2 and Rd-open states (PDB:
557 4AAR and 4AB3, respectively; [23]), and the GroES-bound ES state (PDB: 1SVT; [28]). The binding
558 paratope (shown in sea green) is accessible in the T, Rs, and Rs/Rd-open states, but becomes
559 inaccessible in the GroES-bound ES state. In addition, sterically, the different conformational
560 states of the GroEL apical domain would be compatible with CnoX binding, except for the ES
561 state. CnoX is shown in pink. The GroEL equatorial, intermediate, and apical domains are
562 shown in slate, orange, and light cyan. GroES is shown in fuchsia.

563

564 **Figure S5. The C-terminus of CnoX interacts with human mitochondrial Hsp60 and is**
565 **conserved in eukaryotic proteins sharing structural features with CnoX, related to Figure 4**
566 **(A)** GroEL (lane 1) or mHsp60 (migrates slightly lower than GroEL; lane 2) co-elutes with
567 CnoX when CnoX is pulled down from cell extracts using α-CnoX antibodies. In these
568 experiments, we expressed GroEL and mHsp60 in BL21 (DE3) cells. The SDS-PAGE gel,
569 stained with Coomassie blue, is representative of >3 replicates. * indicates the light and
570 heavy chains of the antibodies.
571 **(B,C,D)** Representative AlphaFold 3D models of eukaryotic homologs of CnoX. B) *Stentor*
572 *coeruleus* (UniProt A0A1R2CPV9), C) *Emiliania huxleyi* (UniProt R1DRS2), and D)
573 *Pseudocohnilembus persalinus* (UniProt A0A0V0QL30). The domains *thioredoxin*, *TPR_19*,
574 and *TPR_20* (colored in blue, green, and red, respectively) of CnoX (PDB code 3QOU) are
575 superposed on these AlphaFold models (colored in gold).

STAR*Methods

RESOURCE AVAILABILITY

Lead contact

Further information and requests for resources and reagents should be directed to and will be fulfilled by the lead contact, Jean-François Collet (jfcollet@uclouvain.be).

Materials availability

Strains and plasmids generated in this study are available upon request to the lead contact.

Data and code availability

- Coordinates and electron potential maps for the GroEL:CnoX cryoEM structure have been deposited in the PDB and EMDB under accession codes 7YWY and EMD-14352, respectively.
- Raw data from Figures 1, 2, 3, 4, 5 and Supplemental Figures 1, 2, 3, 4, 5, 6 were deposited on Mendeley at http://dx.doi.org/10.17632/9pt4v7hc93.1.
- Any additional information required to reanalyze the data reported in this paper is available from the lead contact upon request.

EXPERIMENTAL MODEL AND SUBJECT DETAILS

The *E. coli* strains used in this study are listed in **Table S3**. We prepared the *cnoX* deletion mutant by transferring the corresponding allele (*ybbN*::kan^{R}) from the Keio collection [29] into MG1655 by P1 phage transduction, with verification by polymerase chain reaction (PCR). To excise the kanamycin-resistance cassette, we used pCP20 [30]. Unless otherwise indicated, we grew the cells in lysogeny broth (LB) at 37°C, and when necessary, we supplemented the growth media with ampicillin (100–200 µg/mL), chloramphenicol (100 µg/mL), or kanamycin (50 µg/mL).

METHOD DETAILS

Plasmid construction

Table S4 shows the plasmids used in this study. The primers used for their construction are shown in **Table S5**. To obtain high expression levels of wild-type CnoX, CnoX$_{C\text{-}His}$, GroEL, and GroES, we cloned the corresponding genes into the high copy vector pET22b(+) (Novagen). DNA encoding CnoX$_{N\text{-}Strep}$ was cloned into the medium copy vector pACYCDuet-1. To prepare an expression vector for *cnoX* without the last 10 C-terminal residues (CnoX$_{\Delta Cter}$), we amplified the corresponding sequence from *E. coli* genomic DNA and ligated the sequence into pET22b(+). The CnoX and GroEL substitution variants used in this study were generated by site-directed mutagenesis, except for GroEL$_{G298A/T299L/V300K/E304L/I305K/M307K/R345L}$, which was generated using Gibson assembly. We generated the CnoX$_{N\text{-}link/C38A/C63A}$ variant using site-directed mutagenesis by inserting the coding sequences of Met, Ala, Cys, Ala, and Gly residues at the N-terminal extremity. To prepare an expression vector for mHsp60, we amplified the corresponding sequence from the MAC_C_CH60 vector (Addgene) without the mitochondrial targeting sequence, which was replaced by the coding sequences of Met, Gly, and Ser residues, and cloned the sequence into pET22b(+) using Gibson assembly.

Expression and purification of CnoX, CnoX$_{\Delta Cter}$, CnoX$_{N\text{-}Strep}$, CnoX$_{C\text{-}His}$, and CnoX$_{N\text{-}link/C38A/C63A}$

We utilized *E. coli* BL21 (DE3) carrying pET22b_cnoX, pET22b_cnoX$_{\Delta Cter}$, or pET22b_cnoX$_{N\text{-}link/C38A/C63A}$ to overexpress wild-type CnoX, CnoX$_{\Delta cter}$, or CnoX$_{N\text{-}link/C38A/C63A}$, respectively. Cells grew at 37°C until the optical density at 600 nm (OD$_{600}$) reached 0.5, and then, we added 1 mM IPTG for 3 h to induce protein expression. Cells were pelleted, resuspended in 50 mM

Tris-HCl pH 8, and disrupted with a French press. After centrifugation for 30 min at 40,000*g* at 4°C, the supernatant was filtered through 0.45-µm filters and loaded onto a 5-mL Q-Sepharose HP column (GE Healthcare). We eluted the proteins with a 0%–50% gradient of 1 M NaCl in 50 mM Tris-HCl pH 8. Proteins underwent a second purification step via a HiLoad 16/60 Superdex 75 gel filtration system (GE Healthcare) and were eluted in 10 mM hydroxyethyl piperazineethanesulfonic (HEPES)-KOH pH 8, 100 mM NaCl.

We employed *E. coli* BL21 (DE3) carrying pET22b-cnoX$_{C\text{-}His}$ to overexpress CnoX fused to a C-terminal His-tag (CnoX$_{C\text{-}His}$). Cells grew at 37°C until an OD$_{600}$ of 0.5 was reached, and we added 1 mM IPTG for 3 h to induce protein expression. Cells were pelleted, resuspended in buffer A (NaPi 50 mM pH 8, 300 mM NaCl), and lysed with a French press. After centrifugation for 30 min at 40,000*g* at 4°C, the supernatant was filtered through 0.45-µm filters and loaded on Ni-nitriloacetic acid (NTA) agarose beads (5 mL; IBA Lifesciences) previously equilibrated with buffer A. After washing the resin with buffer A supplemented with 20 mM imidazole, we eluted the proteins with buffer A supplemented with 300 mM imidazole. As a final purification step, we performed size-exclusion chromatography using a HiLoad 16/60 Superdex 75 column (GE Healthcare) with 10 mM HEPES pH 7, 100 mM NaCl.

E. coli BL21 (DE3) cells carrying pACYCDuet-1-cnoX$_{N\text{-}Strep}$ were used to express CnoX fused to an N-terminal Strep-tag (CnoX$_{N\text{-}Strep}$). Cells grew at 37°C until an OD$_{600}$ of 0.5 was reached, and we added 1 mM IPTG for 3 h to induce protein expression. Cells were pelleted, resuspended in buffer B (50 mM Tris-HCl pH 8, 150 mM NaCl), and lysed with a French press. After centrifugation for 30 min at 40,000*g* at 4°C, the supernatant was filtered through 0.45-µm filters and loaded onto a 5-mL Strep-Tactin column (IBA Lifesciences) previously equilibrated in buffer B. After applying a washing step with buffer B, we performed elution with buffer B supplemented with 2.5 mM D-desthiobiotin. We then purified the sample using size-exclusion chromatography on a HiLoad 10/300 Superdex 200 column (GE Healthcare) using buffer B supplemented with 1 mM ethylenediaminetetraacetic acid (EDTA).

Expression and purification of GroEL, GroEL variants, and GroES

We used *E. coli* BL21 (DE3) cells carrying pET22b-groL to overexpress GroEL. Cells grew at 37°C until an OD$_{600}$ of 0.5 was reached, and we added 1 mM IPTG for 3 h to induce protein expression. Cells were pelleted, resuspended in buffer C containing 50 mM Tris-HCl pH 7.4, 1 mM EDTA, and 1 mM DTT, and lysed with a French press. After centrifugation for 30 min at 40,000*g* at 4°C, the supernatant was filtered through 0.45-µm filters, loaded onto a 5-mL DEAE-Sepharose HP column (GE Healthcare), and eluted in a gradient (0%–50%) of 1 M NaCl in buffer C. The second purification step required gel filtration using a HiLoad S200 16/600 column (GE Healthcare) and elution buffer containing 10 mM HEPES-KOH pH 8, 100 mM NaCl, and 1 mM DTT. Finally, we loaded the protein onto a 5-mL Q-Sepharose HP column (GE Healthcare) using a gradient (0%–50%) of 1 M NaCl in buffer C. GroEL$_{D490C}$, GroEL$_{R452A/E461A/S463A/V464A}$, and GroEL$_{G298A/T299L/V300K/E304L/I305K/M307K/R345L}$ (GroEL§) were purified in a similar manner.

We utilized *E. coli* BL21 (DE3) carrying pET22b-groS to overexpress GroES. Cells were grown at 37°C. When an OD$_{600}$ of 0.5 was reached, we added 1 mM IPTG for 3 h to induce protein expression. Cells were pelleted, resuspended in buffer D (30 mM Tris-HCl pH 7.5, 10 mM NaCl, 1 mM EDTA), and lysed with a French press. After centrifugation for 30 min at 40,000*g* at 4°C, the supernatant was filtered (0.45-µm filters), loaded onto a 5-mL DEAE-Sepharose HP column (GE Healthcare), and eluted in a 0%–50% gradient of 1 M NaCl in buffer D. For the second purification step, we loaded the sample onto a 5-mL Q-Sepharose HP column (GE Healthcare) and eluted the proteins with a 0%–50% gradient of 1 M NaCl in 20 mM imidazole pH 5.8. Finally, we loaded the sample onto a gel filtration column (HiLoad S200 26/60 column [GE Healthcare]) equilibrated in buffer D.

For all proteins, we verified the purity via SDS-PAGE with Coomassie staining and concentrated samples using a Vivaspin Turbo (Sartorius) with a 5-kDa molecular-weight cutoff. We assessed protein concentrations by measuring the absorbance at 280 nm using a Varian Cary 50 UV-Vis spectrophotometer.

Reconstitution of the GroEL-CnoX$_{N\text{-}Strep}$ complex

To reconstitute GroEL-CnoX$_{N\text{-}Strep}$, we mixed GroEL (150 µM) in excess (10:1) or with equimolar amounts of CnoX$_{N\text{-}Strep}$ in 500 µL of buffer A. After 15 min at room temperature, the mixture was loaded onto a 1-mL Strep-Tactin column (IBA Lifesciences) previously equilibrated in buffer A. After applying a washing step with buffer A, we performed elution with buffer A supplemented with 2.5 mM D-desthiobiotin.

Expression and purification of the GroEL-CS-CnoX$_{N\text{-}Strep}$ complex

We used *E. coli* BL21 (DE3) cells carrying pACYCDuet-1-cnoX$_{N\text{-}Strep}$ _gltA_groL to overexpress CnoX$_{N\text{-}Strep}$, CS, and GroEL. Cells were grown at 37°C. When an OD$_{600}$ of 0.5 was reached, we added 1 mM IPTG for 4 h to induce protein expression. Cells were pelleted, resuspended in buffer B (50 mM Tris-HCl pH 8, 150 mM NaCl) supplemented with 1 mM EDTA, and lysed with a French press. After centrifugation for 20 min at 17,418*g* at 4°C, the supernatant was filtered through 0.45-µm filters and loaded onto a 2-mL Strep-Tactin column (IBA Lifesciences) previously equilibrated in buffer B. After applying a washing step with buffer B, we performed elution with buffer B supplemented with 2.5 mM D-desthiobiotin. We then purified the sample using size-exclusion chromatography on a HiLoad 10/300 Superdex 200 column (GE Healthcare) using buffer B supplemented with 1 mM EDTA.

In vivo pull-down of CnoX

E. coli MG1655 wild-type, *E. coli* MG1655 Δ*cnoX*, and *E. coli* MG1655 cells carrying pET22b-cnoX, pET22b-cnoX$_{\Delta Cter}$, pET22b-cnoX$_{R277L}$, pET22b-cnoX$_{Y284L}$, or pET22b-cnoX$_{C\text{-}His}$ grew in LB (25 mL) at 37°C in a shaking incubator until the mid-log phase was reached. The cells were then harvested, resuspended in 1 mL of buffer E (50 mM Tris-HCl pH 7.4, 150 mM NaCl, 1 mM EDTA), and sonicated. After a 5-min centrifugation at 16,000*g* at 4°C, we added 5 µL of undiluted rabbit anti-CnoX antibody and 50 µL of protein A/G magnetic beads (Pierce) to the supernatant to immunoprecipitate CnoX; then, we incubated the samples for 30 min on a wheel at room temperature. After three washes with 500 µL of buffer E, CnoX was eluted with 20 µL of 100 mM glycine pH 2.5. We neutralized the samples with 2 µL of 1.5 M Tris-HCl pH 8 before SDS-PAGE analysis and Coomassie staining.

In vitro pull-down of GroEL

We mixed GroEL (5 µM) with equimolar amounts of either CnoX, CnoX$_{\Delta Cter}$, CnoX$_{C\text{-}His}$, or CnoX and unfolded CS in 100 µL of buffer E. After 30 min at room temperature, we immunoprecipitated GroEL by adding 5 µL of undiluted rabbit anti-GroEL antibody and 50 µL of protein A/G magnetic beads (Pierce); samples were incubated for 30 min on a wheel at room temperature. After three washes with buffer E, GroEL was eluted with 20 µL of 100 mM glycine pH 2.5. We then neutralized the samples with 2 µL of 1.5 M Tris-HCl pH 8 before SDS-PAGE analysis and Coomassie staining.

In vitro pull-down of CnoX

CnoX, CnoX$_{\Delta Cter}$, or CnoX$_{C\text{-}His}$ (5 µM) was mixed with equimolar amounts of GroEL in 100 µL of buffer E. After 30 min at room temperature, we immunoprecipitated CnoX by adding 5 µL of undiluted rabbit anti-CnoX antibody and 50 µL of protein A/G magnetic beads (Pierce); then, we incubated the samples for 30 min on a wheel at room temperature. After three washes with buffer E, CnoX was eluted with 20 µL of 100 mM glycine pH 2.5. We neutralized the samples with 2 µL of 1.5 M Tris-HCl pH 8 before SDS-PAGE analysis and Coomassie staining.

Size-exclusion chromatography analysis

To reconstitute GroEL-CnoX, we mixed both proteins using the ratios indicated in the manuscript. After 15 min at room temperature, the sample was loaded onto a Superdex S200 10/300 column equilibrated with buffer E. The fractions corresponding to absorbance peaks at 280 nm were collected and analyzed by gradient (4%–12%) SDS-PAGE.

To determine the impact of GroES addition on the GroEL-CnoX complex, we mixed GroEL (45 µM) with CnoX using the ratios indicated in the manuscript in 1 mL of buffer F (50 mM Tris-HCl pH 8, 150 mM KCl, 10 mM $MgCl_2$, 1 mM DTT, 1 mM EDTA) supplemented with either ADP (1 mM) or AMP-PNP (1 mM). After 15 min at room temperature, GroES was added at a molar ratio of 14:1:14 (GroEL:CnoX:GroES). After 15 min, we loaded the sample onto a Superdex S200 10/300 column equilibrated with buffer A supplemented with ADP (50 µM) or AMP-PNP (50 µM). The column ran at a flow rate of 0.5 mL/min with 1-mL fractions using an AKTA Purifier (Cytiva). Fractions corresponding to absorbance peaks at 280 nm were collected and analyzed by gradient (4%–12%) SDS-PAGE.

To investigate the binding of CS on GroEL, CS (82 µM, Sigma-Aldrich) was unfolded by dilution in 4 M guanidinium chloride and incubated at room temperature for 2 h. To assay binding on GroEL, we mixed GroEL (45 µM) with unfolded CS (CS_{denat}) at a molar ratio of 14:1 GroEL:CS_{denat} in 1 mL of buffer F supplemented with 1 mM ADP. After 15 min at room temperature, GroES was added at a molar ratio of 14:1:14 GroEL:CS_{denat}:GroES; after another 15 min, we loaded the mixture onto a Superdex S200 10/300 column equilibrated with buffer A supplemented with 50 µM ADP. The column ran at a flow rate of 0.5 mL/min with an AKTA Purifier, and 1-mL fractions were collected. The fractions corresponding to absorbance peaks at 280 nm were collected and analyzed by gradient (4%–12%) SDS-PAGE.

Purification of GroEL, GroES, and CnoX for quantitative binding studies

CnoX and GroES were expressed and purified as previously described [18]. Purified proteins had their N-terminal hexahistidine tags removed by thrombin cleavage and were passed again over Ni^{2+}-NTA resin. These proteins were then collected in the flow-through, dialyzed into storage buffer (25 mM HEPES pH 7.5, 100 mM KCl), snap-frozen in 50- to 100-µL aliquots in liquid nitrogen, and stored at -80°C. We verified tag removal by electrospray MS. We induced GroEL expression from pET15b as an untagged protein by removing the sequence between the “CC” of the NcoI site and the “ATG” of the NdeI site using mutagenic PCR primers (see **Table S5**). GroEL lacking any tag- or vector-derived amino acids was expressed by 0.5 mM IPTG induction, and cells were harvested by centrifugation as described. After sonication and centrifugation at 12000*g*, clarified lysate was loaded onto a Macro-Prep High Q resin (Bio-Rad) column, and proteins were eluted over a 0.1–1.1 M NaCl gradient in 25 mM HEPES pH 7.5. The fractions ran on SDS-PAGE gels, and those enriched in GroEL were pooled. We precipitated the crude GroEL fraction by gradually adding finely ground $(NH_4)_2SO_4$ powder to 75% saturation at room temperature and centrifuging the fraction at 20,000*g* for 45 min. The pellet was then dissolved in storage buffer (25 mM HEPES pH 7.5, 100 mM KCl) and dialyzed against storage buffer overnight. GroEL was applied to a Sephacryl S-300 HR gel filtration column and eluted near the void volume due to the large size of the GroEL oligomer. We identified the fractions containing GroEL by SDS-PAGE and then pooled and dialyzed the fractions against 50 mM Tris-HCl pH 7.5, 1 mM EDTA, 30% methanol (Tris-methanol buffer). The pooled GroEL fractions were loaded onto a UNO Q12 anion exchange column (Bio-Rad) and eluted with a gradient of 0–1 M NaCl in Tris-methanol buffer. We identified GroEL-containing fractions by SDS-PAGE, and those lacking any visible contaminants were pooled, dialyzed into storage buffer, concentrated by centrifugation with a 10-kDa molecular-weight cutoff concentrator, snap-frozen in 50- to 100-µL aliquots in liquid nitrogen, and stored at -80°C.

Fluorescent labeling of CnoX

We fluorescently labeled CnoX using FM (Thermo Fisher Scientific) for binding studies. The maleimide moiety of FM is cysteine-reactive and is therefore expected to label the N-terminal

thioredoxin-like domain of CnoX, which contains the only two cysteine residues in the protein, Cys38 and Cys63. A 25-fold molar excess of FM to CnoX in 20 mM sodium phosphate buffer pH 7.2, 150 mM NaCl, and 5 mM EDTA was incubated for 4 h at room temperature in the dark. We then dialyzed the sample using 3.5-kDa-cutoff regenerated cellulose tubing against storage buffer overnight at 4°C to remove any unreacted FM.

We determined the stoichiometry of FM-CnoX labeling via the ratio of absorbance at 495 nm and 280 nm.

$$\text{Labeling stoichiometry} = \frac{\frac{A_{495}}{\varepsilon_{495}^{FM}}}{\frac{\left(A_{280} - \left(A_{495}\ \frac{\varepsilon_{280}^{FM}}{\varepsilon_{495}^{FM}}\right)\right)}{\varepsilon_{280}^{CnoX}}}$$

The calculated ε_{280} for CnoX is 23,000 M^{-1} cm^{-1} (ExPASY), the ε_{495} of FM is 75,000 $M^{-1}cm^{-1}$, and the ratio of FM extinction coefficients at 280 and 495 nm ($\frac{\varepsilon_{280}^{FM}}{\varepsilon_{495}^{FM}}$; sometimes called the correction factor) is 0.3. The labeling stoichiometry is 2.2 FM per CnoX molecule, as expected for the two cysteine residues in the N-terminal thioredoxin domain. FM-CnoX was snap-frozen in liquid nitrogen and stored at -80°C.

Measurement of the CnoX-GroEL binding affinity

We performed fluorescence measurements on a Cary Eclipse fluorescence spectrophotometer (Varian) at room temperature (~22°C). We measured fluorescence emission spectra between 500 and 560 nm with an excitation wavelength of 495 nm. The excitation and emission slits were set to 5 nm, and spectra were recorded at a scan rate of 10 nm/s. To measure the binding of GroEL to FM-CnoX, we titrated 119 µM GroEL into 0.5 µM FM-CnoX in a total volume of 0.5 mL storage buffer. Final GroEL concentrations ranged from 0.035 to 1 µM. We calculated the normalized fluorescence ratio (D) as:

$$D = \frac{F_i}{F_0} - 1$$

where F_i is the fluorescence emission of FM-CnoX at peak (typically 520 nm) measured after the addition of GroEL and F_0 is the fluorescence emission at peak measured for FM-CnoX alone.

To complement the fluorescence emission measurements, we performed a fluorescence anisotropy binding assay using a Jasco J-815 CD spectrophotometer at 20°C. We employed an excitation wavelength of 495 nm and a 540-nm emission filter. Measurements were collected using a cell with a 1-cm path length at a scan rate of 0.833 nm/s from 450 to 550 nm. In a total volume of 2 mL of storage buffer, we titrated 0.5 µM FM-CnoX with 119 µM GroEL to final concentrations ranging from 0.036 to 1 µM. The final volume change after GroEL titration was less than 1%. We measured the fluorescence anisotropy for each titration point 2 min after the addition of GroEL. The data were averaged from 3–4 measurements. Binding data were plotted and fitted in Prism (GraphPad) using nonlinear least-squares minimization. We utilized a single-site binding model with positive cooperativity for the CnoX-GroEL interactions and a single-site competition model with a logarithmic competitor concentration for the GroES competition experiment. No data linearization was performed.

Influence of nucleotides on the CnoX-GroEL and GroES interaction

To examine the effect of ATP or ADP on GroEL-CnoX binding, we repeated the experiment described in the previous section using 0.5 µM FM-CnoX and GroEL in storage buffer with 2 mM ATP (Alfa Aesar) or 2 mM ADP (Sigma) and 10 mM $MgCl_2$. For the GroES competition

experiment, 0.5 µM FM-CnoX was incubated with 0.5 µM GroEL, with or without 2 mM ATP in storage buffer, and then titrated with GroES to final concentrations ranging from 0.035 to 2 µM. We measured the fluorescence emission at peak 2 min after adding titrated protein at room temperature. In all titrations, the final volume change was less than 1%; hence, no dilution correction was performed. Data were averaged from 3–4 measurements.

In vivo trapping of GroEL-CnoX-substrate tripartite complexes

To identify proteins trapped in a mixed disulfide with CnoX when CnoX is bound to GroEL, we immunoprecipitated GroEL from extracts prepared from *E. coli* BL21 (DE3) cells carrying pET22b-cnoX and pET22b-cnoX$_{C38A/C63A}$ as follows. After an overnight preculture, cells were diluted in 500 mL of LB containing 100 mg/mL ampicillin and grown at 37°C. At the mid-log phase, we induced protein expression for 1 h with 1 mM IPTG. Cultures were cooled on ice for 10 min, and iodoacetamide (25 mM) was added. After 30 min, the cells were harvested, resuspended in 20 mL of buffer E, and sonicated. After performing centrifugation at 12,000*g* at 4°C, we added 150 µL of undiluted rabbit anti-GroEL antibody and 1 mL of protein A/G magnetic beads (Pierce) to the supernatant. After 30 min on a wheel at room temperature, magnetic beads were collected and resuspended with 1 mL of buffer E. After applying three washes with 1 mL of buffer E, we eluted GroEL with 100 µL of 0.1 M glycine pH 2.5.

Chaperone-mediated reactivation of chemically unfolded CS

We adapted our protocol from Haslbeck and Buchner (2015) and Hoffmann et al. (2004). Briefly, 15 mM CS (Sigma-Aldrich) was unfolded by dilution in 4 M guanidinium chloride in Tris-EDTA buffer (50 mM Tris-HCl [pH 8], 2 mM EDTA) and incubated at 16°C for 2 h. We diluted the unfolded CS by 1:160 (final concentration of 75 nM) in 40 mM HEPES-KOH (pH 8), 10 mM KCl, and 2 mM Mg-ATP (unless otherwise specified) containing 0 or 0.45 mM YbbN. After a 20-min incubation at 25°C, the DnaK/DnaJ/GrpE refolding system (0.4 mM, 0.16 mM, and 0.4 mM, respectively) or the GroEL14/GroES7 refolding system (0.15 mM and 0.5 mM, respectively) was added to the refolding solution and incubated for 2 h at 25°C. We added 4 mL of this mixture to 200 mL of reaction buffer (100 mM oxaloacetic acid, 100 mM 5,5'-dithiobis(2-nitrobenzoic acid), and 160 mM acetylCoA in Tris-EDTA buffer) in a 96-well plate. We monitored the absorbance at 412 nm for 1 min with a Biotek Synergy H1 Hybrid microplate reader and used the initial slope of the absorbance values to calculate the CS activity.

Bacterial viability assay

E. coli MC4100 Δ*tig*Δ*dnaKdnaJ* cells carrying p29SEN-EV, p29SEN-groSgroL, p29SEN-groSgroL$_{heptuple}$, p29SEN-groSgroLcnoX, or p29SEN-groSgroLcnoX$_{\Delta Cter}$ grew in LB supplemented with ampicillin at 20°C until the mid-log phase was reached. Cells were serially diluted and spotted on LB agar plates containing ampicillin, with or without 100 µM IPTG, overnight at 37°C.

AFM

Gold-coated glass coverslips and cantilevers (OMCL-TR4, Olympus Ltd.; nominal spring constant of ~0.02 N m^{-1}) were incubated with 0.1 mg mL^{-1} of CnoX$_{N\text{-}link/C38A/C63A}$, the last C-terminal 10 amino acids of CnoX fused to a linker (CGGGSGGGYRRQLYALLY), or GroEL$_{D490C}$ solution for 1 h, rinsed with buffer D, and then immediately used without dewetting. We performed measurements at room temperature in 50 mM Tris pH 8, 150 mM NaCl, 1 mM EDTA with a Force Robot 300 AFM (JPK Instruments). We recorded multiple (32 × 32) force–distance curves over an area of 500 x 500 nm^2 with an applied force of 250 pN, a constant approach, and a retraction speed of 1,000 nm s^{-1}. A histogram was generated based on the force of the last rupture event for each curve. We measured the spring constants of the cantilevers by the thermal noise method and analyzed these data with data-processing software from JPK Instruments.

Native PAGE

We performed Blue native electrophoresis analysis of the concentrated complex on a 3%–12% Bis-Tris gel (Life Technologies) following the manufacturer's instructions. We identified the protein complex bands separated in the native electrophoresis via SDS-PAGE. Briefly, bands of interest were excised, boiled in SDS-PAGE sample buffer, and applied to the top of a polyacrylamide gel.

Immunoblotting

Samples were boiled before being loaded onto a precast NuPAGE Bis-Tris 12% gel (Life Technologies). We performed immunoblotting according to standard procedures using 1:5000 anti-CnoX antibody (rabbit serum, CER group, Belgium) followed by a horseradish peroxidase-conjugated anti-rabbit antibody (Sigma). We conducted chemiluminescence imaging (ECL Prime Western Blotting Detection Reagents; GE Healthcare) with an ImageQuant LAS 500 Camera (GE Healthcare Life Sciences).

Mammalian homologs of CnoX

The CnoX structure (http://pfam.xfam.org/protein/P77395) is organized into three domains, corresponding to the Pfam entries *Thioredoxin* (http://pfam.xfam.org/family/Thioredoxin), *TPR_19* (http://pfam.xfam.org/family/TPR_19), and *TPR_20* (http://pfam.xfam.org/family/TPR_20). As of March 9, 2022, these Pfams contain 40,361 (*Thioredoxin*), 10,056 (*TPR_19*), and 44 (*TPR_20*) eukaryotic sequences. We downloaded all 44 eukaryotic sequences from UniProt [31] and built corresponding AlphaFold 3D models using ColabFold [32]. Most of these models contained all three domains (*Thioredoxin*, *TPR_19*, and *TPR_20*). Three representative structures are shown in **Figure S5**.

Protein identification by MS

After in-gel digestion with trypsin, peptides were dissolved in solvent A (0.1% trifluoroacetic acid in 2% acetonitrile), directly loaded onto a reversed-phase precolumn (Acclaim PepMap 100, Thermo Fisher Scientific), and eluted in backflush mode. We performed peptide separation using a reversed-phase analytical column (Acclaim PepMap RSLC, 0.075 x 250 mm, Thermo Fisher Scientific) with a linear gradient of 4%–27.5% solvent B (0.1% formic acid in 98% acetonitrile) for 40 min, 27.5%–50% solvent B for 20 min, 50%–95% solvent B for 10 min, and holding at 95% for the last 10 min at a constant flow rate of 300 nL/min on an Ultimate 3000 RSLC system. We analyzed the peptides by an Orbitrap Fusion Lumos tribrid MS (Thermo Fisher Scientific). The peptides were subjected to a nanospray ionization source followed by MS/MS in a Fusion Lumos coupled online to a nano-LC. Intact peptides were detected in the Orbitrap at a resolution of 120,000. We selected peptides for MS/MS using a higher-energy collision dissociation setting of 30 and detected ion fragments in the Orbitrap at a resolution of 30,000. A data-dependent procedure that alternated between one MS scan and one MS/MS scan was applied for 3 s for ions above a threshold ion count of 2.0×10^4 in the MS survey scan with 40.0-s dynamic exclusion. An electrospray voltage of 2.1 kV was applied. We obtained MS1 spectra with an automatic gain control target of 4×10^5 ions and a maximum injection time of 50 ms and MS2 spectra with an automatic gain control target of 5×10^4 ions and a maximum injection set to dynamic. For MS scans, the m/z scan range was 375–1800. We processed the resulting MS/MS data using the Sequest HT search engine within Proteome Discoverer 2.4 SP1 against an *E. coli K12* protein database obtained from Uniprot (4,349 entries). Trypsin was specified as a cleavage enzyme allowing up to two missed cleavages, four modifications per peptide, and up to five charges. We set the mass error to 10 ppm for precursor ions and 0.1 Da for fragment ions. Oxidation on Met (+15.995 Da) and conversion of Gln (-17.027 Da) or Glu (-18.011 Da) to pyro-Glu at the peptide N-terminal were considered as variable modifications. We assessed the false discovery rate using Percolator, with the thresholds for proteins, peptides, and modification sites specified at 1%. For abundance comparison, we calculated abundance ratios by label-free quantification of the precursor intensities within Proteome Discoverer 2.4 SP1.

Crosslinking identification by MS

We applied 100 µL of the purified ternary complex between CS, CnoX, and GroEL onto a NAP-5 column for buffer exchange into 500 µL of 20 mM HEPES pH 8. Then, DSSO was not added or added to the protein sample at a final concentration of 2 mM. After 60 min at room temperature, we ended the reaction by adding 40 mM of Tris pH 8. Protein extraction and digestion with trypsin were performed as in [33]. Briefly, protein samples were precipitated by adding three volumes of methanol, one volume of chloroform, and three volumes of water, vortexed, and centrifuged at 15,000*g* for 2 min at room temperature. The supernatant was removed carefully and the precipitated protein layers at the interface were further washed and pelleted by adding three volumes of methanol and centrifuging at 15,000*g* for 2 min. Subsequently, the protein pellets were air-dried for 10 min after removing the methanol. The protein pellets were then resuspended in 200 µL of a buffer containing 4 M urea, 50 mM NH_4HCO_3 and sonicated at 80 % amplitude (20 kHz) for 30 s. The protein suspension was reduced by 5 mM tris(2-carboxyethyl)-phosphine (TCEP) at 55 °C for 20 min and then alkylated by 10 mM iodoacetamide in the dark at 25 °C for 20 min with vigorous shaking using a Thermomixer Eppendorf Comfort at 1000 rpm. Afterwards, the proteins were digested by adding 250 µL 50 mM NH_4HCO_3, 2.5 µL 1 % ProteaseMAX™ Surfactant dissolved in 50 mM NH_4HCO_3, and 1:100 (enzyme/protein, w/w) Sequencing Grade Modified Trypsin to reach a final reaction volume of 500 µL. The digestion reactions were incubated overnight at 37 °C with vigorous shaking using a Thermomixer Eppendorf Comfort. The next day, the protein digestion reactions were stopped by adding trifluoroacetic acid (TFA) to 0.1 % final concentration. We then conducted size-exclusion enrichment of crosslinked peptides on a Vivaspin membrane with a 5-kDa cutoff (Sartorius). Peptide separation was performed on an Ultimate 3000-nLC RSLC essentially as described in [33] except that the analytical column was a C18 reversed-phase nano-analytical column (BioZen Polar-C18, 250 x 0.075 mm, Phenomenex). We subjected the peptides to a nanospray ionization source followed by tandem MS/MS in a tribrid Fusion Lumos Orbitrap analyzer coupled online to a nano-LC. Spectra were acquired by an XLMS Clevable MS2-MS3 scan routine specific for DSSO Xlinks with MS1 and MS2 detection in the Orbitrap and MS3 in the Ion Trap. In summary, we acquired full MS1 spectra at a resolution of 120,000 and MS2 scans at a resolution of 30,000. The first MS2 scan was performed in data-dependent acquisition mode with collision-induced dissociation (CID) fragmentation and analysis of the daughter ions in the Orbitrap. If a targeted mass difference specific for DSSO (31.9721 Da) was detected in an ion pair, this finding would trigger a supplemental MS2 fragmentation of the same parent ion by EThcD and several MS3 scans for both ions in the pair by CID fragmentation. We processed the resulting MS/MS data using Sequest HT and the Xlink 2.5 search engine within Proteome Discoverer 2.5 against an *E. Coli* protein database obtained from Uniprot (4,353 entries) and a specific homemade library containing six proteins (groEL, cnoX, tufB, ompA, gltA, lpp) for Xlink identification. Trypsin was specified as a cleavage enzyme allowing up to two missed cleavages, four modifications per peptide, and up to seven charges. We set the mass error to 10 ppm for precursor ions and 0.02 Da for fragment ions. Oxidation on methionine, carbamidomethyl on cysteine, and DSSO monolinks were considered as variable modifications. We assessed the false discovery rate using Percolator and set specified thresholds for proteins, peptides, and modification sites at 1%.

Single-particle cryoEM imaging and data processing

Prior to vitrification, we assessed the sample quality using negative-stain EM. For this step, 3 µL GroEL-CnoX at 0.4 mg/mL was applied to a glow-discharged formvar Cu400 grid (Electron Microscopy Sciences) and screened using in-house 120-kV JEOL JEM 1400 and 1400+ microscopes equipped with an LaB_6 filament at the VIB-VUB BECM facility. We vitrified the GroEL-CnoX sample in liquid ethane using a CP3 Cryoplunge (Gatan) set to 100% humidity and room temperature. R2/1 (Quantifoil) grids were coated with graphene oxide (Sigma), and a 3-µL sample at 0.4 mg/mL was applied and manually back-blotted for 4 s before plunging.

We collected data on an in-house (BECM) 300-kV JEOL CRYOARM 300 equipped with a K3 direct electron detector (Gatan). We collected 3,015 movies in counting mode, with a dose of

68.27 e/Å^2 spread over 61 frames at a nominal magnification of 60.000X, corresponding to a pixel size of 0.784 Å. Images were motion-corrected via MotionCor2.1 [34] using 5 x 5 patches with dose-weighting, and the contrast transfer function was estimated using ctffind4.1 [35]. We picked particles using crYOLO 1.5 [36] with a dataset-specific trained crYOLO network on six micrographs (709 picked particles). The picking quality and CnoX occupancy were assessed using ISAC2 [37] as implemented in the SPHIRE package [38].

We performed all subsequent processing using RELION3.0 [39]. A total of 670,080 picked particles were extracted with a box size of 400 and were binned twice for processing. A c1 initial 3D model was generated *ab initio*. In all subsequent steps, we applied c7 symmetry throughout. After extensive rounds of 3D classification to optimize the density for CnoX on GroEL, we utilized 170,458 particles for the final reconstruction at 3.4 Å.

Final maps were density-modified using phenix.resolve [40], and the model was fitted and symmetry-expanded in UCSF Chimera [41] using the second TPR domain of CnoX (helices 2_A-2_A'-2_B-2_B'-2_C [197-284] from PDB: 3QOU) and GroEL (pdb:1XCK) as starting coordinates. We conducted further docking and refinement using phenix.real.space [42] with manual curation in COOT.[43] After the first refinement, we generated a second local resolution-sharpened map using LocScale [44], as implemented in the CCPEM project package [45]. We used this map together with the density-modified map to aid further map building and refinement in Phenix [46]. The reported FSC-model curve, resolution, and local-resolution maps were calculated using the Phenix validation output and the Phenix implementation of local-resolution assessment.

QUANTIFICATION AND STATISTICAL ANALYSIS

We performed statistical analysis using GraphPad Prism 6. Results are represented as the mean ± standard error of the mean. We conducted comparisons of two groups using unpaired two-tailed Student's t-tests with an assumed Gaussian distribution and equal variances. Experiments were performed in triplicate (n = 3) unless otherwise indicated.

REFERENCES

1. Anfinsen, C.B. (1973). Principles that govern the folding of protein chains. Science *181*, 223-230.
2. Jahn, T.R., and Radford, S.E. (2005). The Yin and Yang of protein folding. The FEBS journal *272*, 5962-5970.
3. Ellis, R.J. (2001). Macromolecular crowding: obvious but underappreciated. Trends in biochemical sciences *26*, 597-604.
4. Hartl, F.U., Bracher, A., and Hayer-Hartl, M. (2011). Molecular chaperones in protein folding and proteostasis. Nature *475*, 324-332. 10.1038/nature10317.
5. Goloubinoff, P., Christeller, J.T., Gatenby, A.A., and Lorimer, G.H. (1989). Reconstitution of active dimeric ribulose bisphosphate carboxylase from an unfolded state depends on two chaperonin proteins and Mg-ATP. Nature *342*, 884-889.
6. Horwich, A.L., and Fenton, W.A. (2020). Chaperonin-assisted protein folding: a chronologue. Quarterly reviews of biophysics *53*.
7. Hayer-Hartl, M., Bracher, A., and Hartl, F.U. (2016). The GroEL–GroES chaperonin machine: a nano-cage for protein folding. Trends in biochemical sciences *41*, 62-76.
8. Hohn, T., Hohn, B., Engel, A., Wurtz, M., and Smith, P.R. (1979). Isolation and characterization of the host protein groE involved in bacteriophage lambda assembly. Journal of molecular biology *129*, 359-373.
9. Hendrix, R.W. (1979). Purification and properties of groE, a host protein involved in bacteriophage assembly. Journal of molecular biology *129*, 375-392.
10. Braig, K., Otwinowski, Z., Hegde, R., Boisvert, D.C., Joachimiak, A., Horwich, A.L., and Sigler, P.B. (1994). The crystal structure of the bacterial chaperonln GroEL at 2.8 Å. Nature *371*, 578-586.
11. Chandrasekhar, G.N., Tilly, K., Woolford, C., Hendrix, R., and Georgopoulos, C. (1986). Purification and properties of the groES morphogenetic protein of Escherichia coli. Journal of Biological Chemistry *261*, 12414-12419.
12. Hunt, J.F., Weaver, A.J., Landry, S.J., Gierasch, L., and Deisenhofer, J. (1996). The crystal structure of the GroES co-chaperonin at 2.8 Å resolution. Nature *379*, 37-45.
13. Xu, Z., Horwich, A.L., and Sigler, P.B. (1997). The crystal structure of the asymmetric GroEL–GroES–(ADP) 7 chaperonin complex. Nature *388*, 741-750.
14. Langer, T., Pfeifer, G., Martin, J., Baumeister, W., and Hartl, F.-U. (1992). Chaperonin-mediated protein folding: GroES binds to one end of the GroEL cylinder, which accommodates the protein substrate within its central cavity. The EMBO journal *11*, 4757-4765.
15. Martin, J., Mayhew, M., Langer, T., and Hartl, U. (1993). The reaction cycle of GroEL and GroES in chaperonin-assisted protein folding. Nature *366*, 228-233.
16. Goemans, C.V., Vertommen, D., Agrebi, R., and Collet, J.-F. (2018). CnoX is a chaperedoxin: a holdase that protects its substrates from irreversible oxidation. Molecular cell *70*, 614-627. e617.
17. Goemans, C.V., Beaufay, F., Arts, I.S., Agrebi, R., Vertommen, D., and Collet, J.-F. (2018). The chaperone and redox properties of CnoX chaperedoxins are tailored to the proteostatic needs of bacterial species. mBio *9*, e01541-01518.
18. Lin, J., and Wilson, M.A. (2011). Escherichia coli thioredoxin-like protein YbbN contains an atypical tetratricopeptide repeat motif and is a negative regulator of GroEL. Journal of Biological Chemistry *286*, 19459-19469.

19. Li G-W, B.D., Gross CA, Weissman JS (2014). Quantifying absolute protein synthesis rates reveals principles underlying allocation of cellular resources. . Cell *157*, 624–635.
20. Weissman, J.S., Hohl, C.M., Kovalenko, O., Kashi, Y., Chen, S., Braig, K., Saibil, H.R., Fenton, W.A., and Norwich, A.L. (1995). Mechanism of GroEL action: productive release of polypeptide from a sequestered position under GroES. Cell *83*, 577-587.
21. Genevaux, P., Keppel, F., Schwager, F., Langendijk-Genevaux, P.S., Hartl, F.U., and Georgopoulos, C. (2004). In vivo analysis of the overlapping functions of DnaK and trigger factor. EMBO reports *5*, 195-200.
22. Brinker, A., Scheufler, C., Von Der Mulbe, F., Fleckenstein, B., Herrmann, C., Jung, G., Moarefi, I., and Hartl, F.U. (2002). Ligand discrimination by TPR domains. Relevance and selectivity of EEVD-recognition in Hsp70 x Hop x Hsp90 complexes. J Biol Chem *277*, 19265-19275. 10.1074/jbc.M109002200.
23. Clare, D.K., Vasishtan, D., Stagg, S., Quispe, J., Farr, G.W., Topf, M., Horwich, A.L., and Saibil, H.R. (2012). ATP-triggered conformational changes delineate substrate-binding and-folding mechanics of the GroEL chaperonin. Cell *149*, 113-123.
24. Ewalt, K.L., Hendrick, J.P., Houry, W.A., and Hartl, F.U. (1997). In vivo observation of polypeptide flux through the bacterial chaperonin system. Cell *90*, 491-500.
25. Imlay, J.A. (2008). Cellular defenses against superoxide and hydrogen peroxide. Annu. Rev. Biochem. *77*, 755-776.
26. Ezraty, B., Gennaris, A., Barras, F., and Collet, J.F. (2017). Oxidative stress, protein damage and repair in bacteria. Nat Rev Microbiol *15*, 385-396. 10.1038/nrmicro.2017.26.
27. Fujiwara, K., Ishihama, Y., Nakahigashi, K., Soga, T., and Taguchi, H. (2010). A systematic survey of in vivo obligate chaperonin-dependent substrates. EMBO J *29*, 1552-1564. 10.1038/emboj.2010.52.
28. Chaudhry, C., Horwich, A.L., Brunger, A.T., and Adams, P.D. (2004). Exploring the structural dynamics of the E. coli chaperonin GroEL using translation-libration-screw crystallographic refinement of intermediate states. Journal of molecular biology *342*, 229-245.
29. Baba, T., Ara, T., Hasegawa, M., Takai, Y., Okumura, Y., Baba, M., Datsenko, K.A., Tomita, M., Wanner, B.L., and Mori, H. (2006). Construction of Escherichia coli K-12 in-frame, single-gene knockout mutants: the Keio collection. Mol Syst Biol *2*, 2006 0008. msb4100050 [pii]
10.1038/msb4100050.
30. Cherepanov, P.P., and Wackernagel, W. (1995). Gene disruption in Escherichia coli: TcR and KmR cassettes with the option of Flp-catalyzed excision of the antibiotic-resistance determinant. Gene *158*, 9-14.
31. Consortium, U. (2021). Bateman A., Martin M. J., Orchard S., Magrane M., Agivetova R., Ahmad S., Alpi E., Bowler-Barnett EH, Britto R., et al. UniProt: The universal protein knowledgebase in.
32. Mirdita, M., Schütze, K., Moriwaki, Y., Heo, L., Ovchinnikov, S., and Steinegger, M. (2022). ColabFold: making protein folding accessible to all. Nature Methods, 1-4.
33. Luo, T., Pueyo, J.M., Wahni, K., Yvanoff, C., Lazar, T., dit Ruys, S.P., Vertommen, D., Ezeriņa, D., and Messens, J. (2021). Thiol-disulphide independent in-cell trapping for the identification of peroxiredoxin 2 interactors. Redox biology *46*, 102066.

34. Zheng, S.Q., Palovcak, E., Armache, J.-P., Verba, K.A., Cheng, Y., and Agard, D.A. (2017). MotionCor2: anisotropic correction of beam-induced motion for improved cryo-electron microscopy. Nature methods *14*, 331-332.
35. Rohou, A., and Grigorieff, N. (2015). CTFFIND4: Fast and accurate defocus estimation from electron micrographs. Journal of structural biology *192*, 216-221.
36. Wagner, T., Merino, F., Stabrin, M., Moriya, T., Antoni, C., Apelbaum, A., Hagel, P., Sitsel, O., Raisch, T., and Prumbaum, D. (2019). SPHIRE-crYOLO is a fast and accurate fully automated particle picker for cryo-EM. Commun. Biol. 2. Nature Publishing Group.
37. Yang, Z., Fang, J., Chittuluru, J., Asturias, F.J., and Penczek, P.A. (2012). Iterative stable alignment and clustering of 2D transmission electron microscope images. Structure *20*, 237-247.
38. Moriya, T., Saur, M., Stabrin, M., Merino, F., Voicu, H., Huang, Z., Penczek, P.A., Raunser, S., and Gatsogiannis, C. (2017). High-resolution single particle analysis from electron cryo-microscopy images using SPHIRE. JoVE (Journal of Visualized Experiments), e55448.
39. Zivanov, J., Nakane, T., Forsberg, B.O., Kimanius, D., Hagen, W.J., Lindahl, E., and Scheres, S.H. (2018). New tools for automated high-resolution cryo-EM structure determination in RELION-3. elife *7*, e42166.
40. Terwilliger, T.C., Ludtke, S.J., Read, R.J., Adams, P.D., and Afonine, P.V. (2020). Improvement of cryo-EM maps by density modification. Nature Methods *17*, 923-927.
41. Pettersen, E.F., Goddard, T.D., Huang, C.C., Couch, G.S., Greenblatt, D.M., Meng, E.C., and Ferrin, T.E. (2004). UCSF Chimera—a visualization system for exploratory research and analysis. Journal of computational chemistry *25*, 1605-1612.
42. Afonine, P.V., Poon, B.K., Read, R.J., Sobolev, O.V., Terwilliger, T.C., Urzhumtsev, A., and Adams, P.D. (2018). Real-space refinement in PHENIX for cryo-EM and crystallography. Acta Crystallographica Section D: Structural Biology *74*, 531-544.
43. Emsley, P., and Cowtan, K. (2004). Acta Crystallographica, Section D: Biological Crystallography. Acta Crystallographica, Section D: Biological Crystallography *60*, 2126-2132.
44. Jakobi, A.J., Wilmanns, M., and Sachse, C. (2017). Model-based local density sharpening of cryo-EM maps. Elife *6*, e27131.
45. Burnley, T., Palmer, C.M., and Winn, M. (2017). Recent developments in the CCP-EM software suite. Acta Crystallographica Section D: Structural Biology *73*, 469-477.
46. Liebschner, D., Afonine, P.V., Baker, M.L., Bunkóczi, G., Chen, V.B., Croll, T.I., Hintze, B., Hung, L.-W., Jain, S., and McCoy, A.J. (2019). Macromolecular structure determination using X-rays, neutrons and electrons: recent developments in Phenix. Acta Crystallographica Section D: Structural Biology *75*, 861-877.
47. Emsley, P., and Cowtan, K. (2004). Coot: model-building tools for molecular graphics. Acta Crystallogr D Biol Crystallogr *60*, 2126-2132. S0907444904019158 [pii] 10.1107/S0907444904019158.
48. Schneider, C.A., Rasband, W.S., and Eliceiri, K.W. (2012). NIH Image to ImageJ: 25 years of image analysis. Nature methods *9*, 671-675.

KEY RESOURCES TABLE

REAGENT or RESOURCE	SOURCE	IDENTIFIER
Antibodies		
Polyclonal rabbit anti-YbbN (CnoX)	CER group, Belgium	Goemans et al., 2018
Polyclonal rabbit anti-GroEL	CER group, Belgium	This study
Anti-rabbit	Sigma	A6154-1ml
Bacterial and virus strains		
E. coli K-12 strain MG1655 (wild type)	JFC lab	N/A
E. coli K-12 strain MC4100	Genevaux lab	N/A
E. coli B strain BL21 (DE3)	JFC lab	N/A
All other strains (Table S3)	This study	This study
Chemicals, peptides, and recombinant proteins		
Ampicillin	Sigma-Aldrich	10835242001
Kanamycin	Sigma-Aldrich	70560-51-9
Chloramphenicol	Sigma-Aldrich	56-75-7
Citrate synthase (CS) from pig hearts	Sigma-Aldrich	C3260
Isopropyl β-D-1-thiogalactopyranoside (IPTG)	Sigma-Aldrich	10724815001
Dithiothreitol (DTT)	Sigma-Aldrich	10197777001
Fluorescein-5-maleimide (FM)	Thermo Fisher	62245
Adenylyl-imidodiphosphate (AMP-PNP)	Sigma-Aldrich	10102547001
Adenosine 5′-diphosphate	Sigma-Aldrich	A2754
Pierce Protein A/G Magnetic Beads	Thermo Fisher	88803
Disuccinimidyl sulfoxide (DSSO)	Thermo Fisher	A33545
ProteaseMAX™ Surfactant	Promega	V2071
Sequencing Grade Modified Trypsin	Promega	V5111
Deposited data		
GroEL-CnoX structure	This study	EMD-14352, PDB: 7YWY
MS-proteomics data	This study and Proteomics Identification Database	N/A
Raw data	Mendeley table	http://dx.doi.org/10.17632/9pt4v7hc93.1
Oligonucleotides		
See Table S5	This study	N/A
Recombinant DNA		
See Table S4	This study	N/A
Software and algorithms		
UCSF Chimera	[41]	https://www.cgl.ucsf.edu/chimera/
ColabFold	[32]	N/A
MotionCor2.1	[34]	N/A
ctffind4.1	[35]	N/A
crYOLO 1.5	[36]	N/A
ISAC2	[37]	N/A

RELION3.0	[39]	N/A
phenix.resolve	[40]	N/A
phenix.real.space	[42]	N/A
COOT	[47]	N/A
LocScale	[44]	N/A
CCPEM project package	[45]	N/A
Phenix	[46]	N/A
ImageJ	[48]	N/A
Image Lab	https://www.bio-rad.com/en-be/product/image-lab-software	N/A

Figure 1

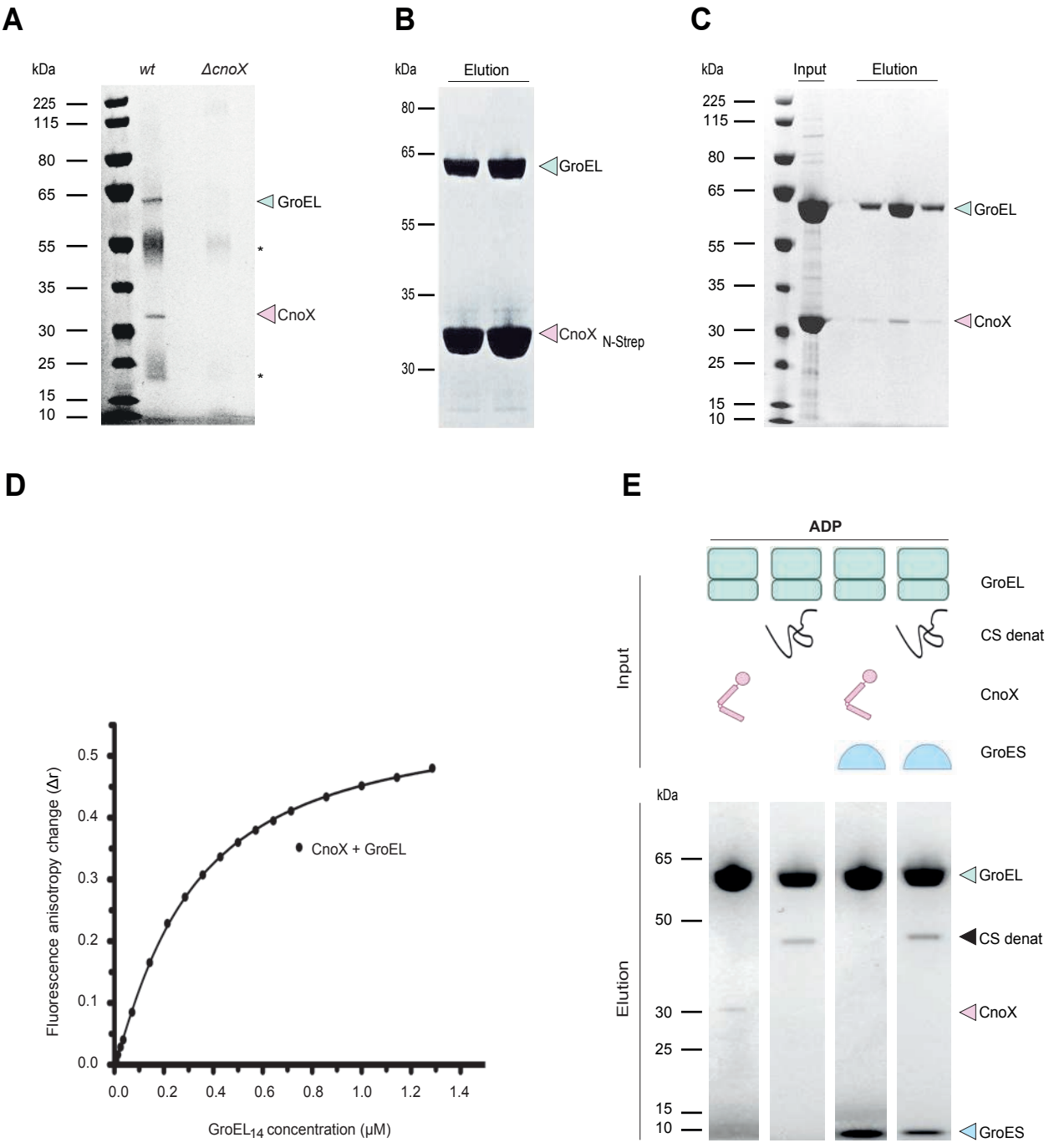
A
kDa
wt
ΔcnoX
225
115
80
65
55
35
30
25
15
10
GroEL
*
CnoX
*
B
kDa
Elution
80
65
55
35
30
GroEL
CnoX N-Strep
C
kDa
Input
Elution
225
115
80
65
55
35
30
25
15
10
GroEL
CnoX
D
Fluorescence anisotropy change (Δr)
0.5
0.4
0.3
0.2
0.1
0.0
CnoX + GroEL
0.0
0.2
0.4
0.6
0.8
1.0
1.2
1.4
GroEL14 concentration (μM)
E
ADP
Input
GroEL
CS denat
CnoX
GroES
kDa
Elution
65
50
30
25
15
10
GroEL
CS denat
CnoX
GroES

Figure 2

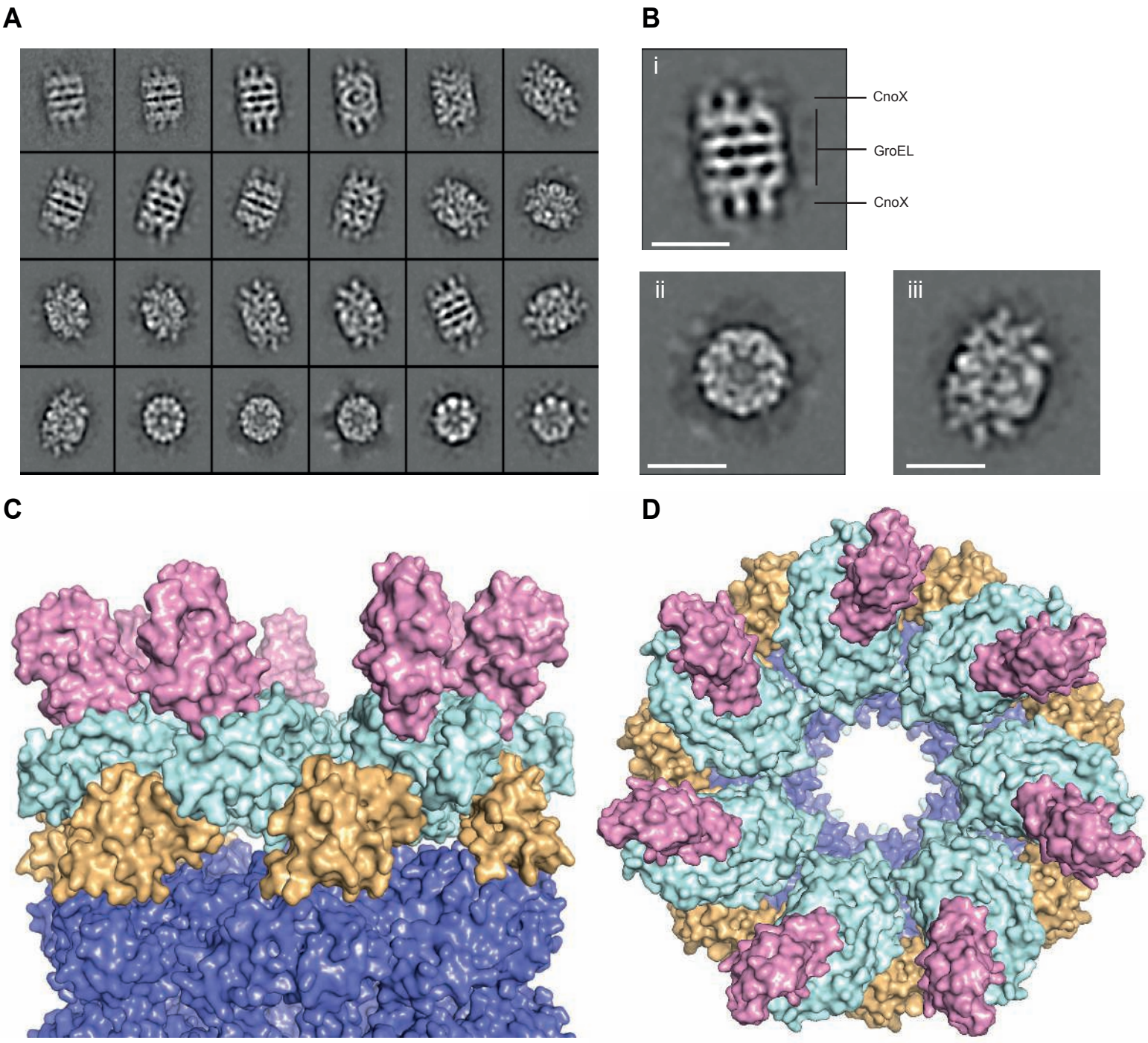

Figure 3

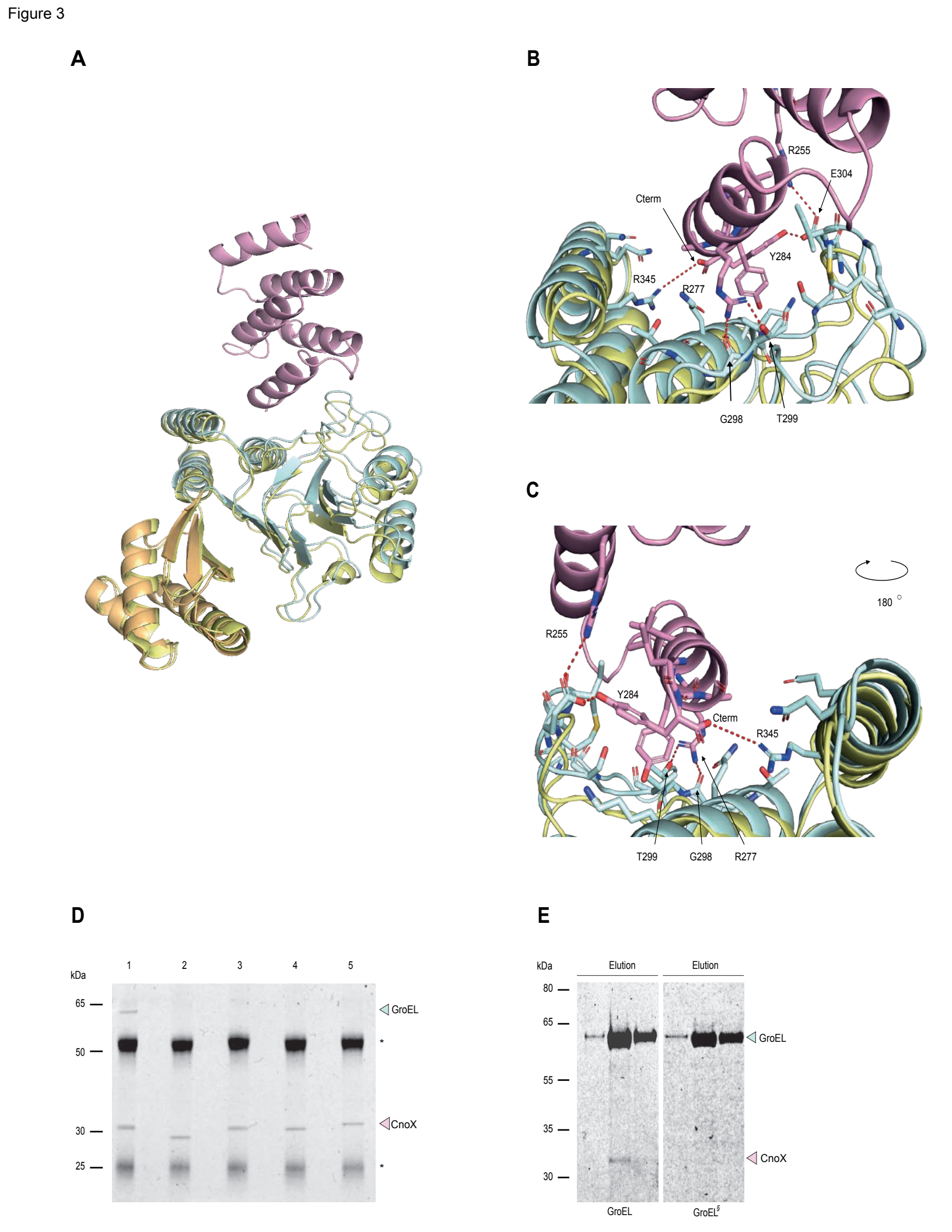
A
B
R255
E304
Cterm
Y284
R345
R277
G298
T299
C
180 °
R255
Y284
Cterm
R345
T299
G298
R277
D
kDa
1
2
3
4
5
65
50
30
25
GroEL
*
CnoX
*
E
kDa
Elution
Elution
80
65
55
35
30
GroEL
CnoX
GroEL
GroEL$^{\delta}$

Figure 4

A

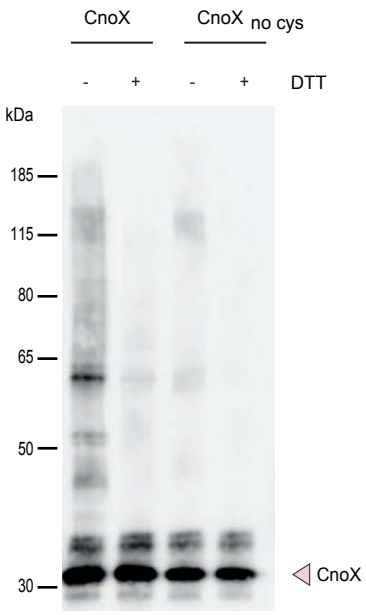

B

Accession #	Protein	Gene
P23908	Acetylornithine deacetylase	argE
P0A6L2	4-hydroxy-tetrahydrodipicolinate synthase	dapA
P0AAI5	3-oxoacyl-[acyl-carrier-protein] synthase 2	fabF
P00370	NADP-specific glutamate dehydrogenase	gdhA
P0ACB2	Delta-aminolevulinic acid dehydratase	hemB
P0A817	S-adenosylmethionine synthase	metK
P0AC41	Succinate dehydrogenase flavoprotein subunit	sdhA
P23721	Phosphoserine aminotransferase	serC
P0AGG8	Metalloprotease TldD	tldD

C

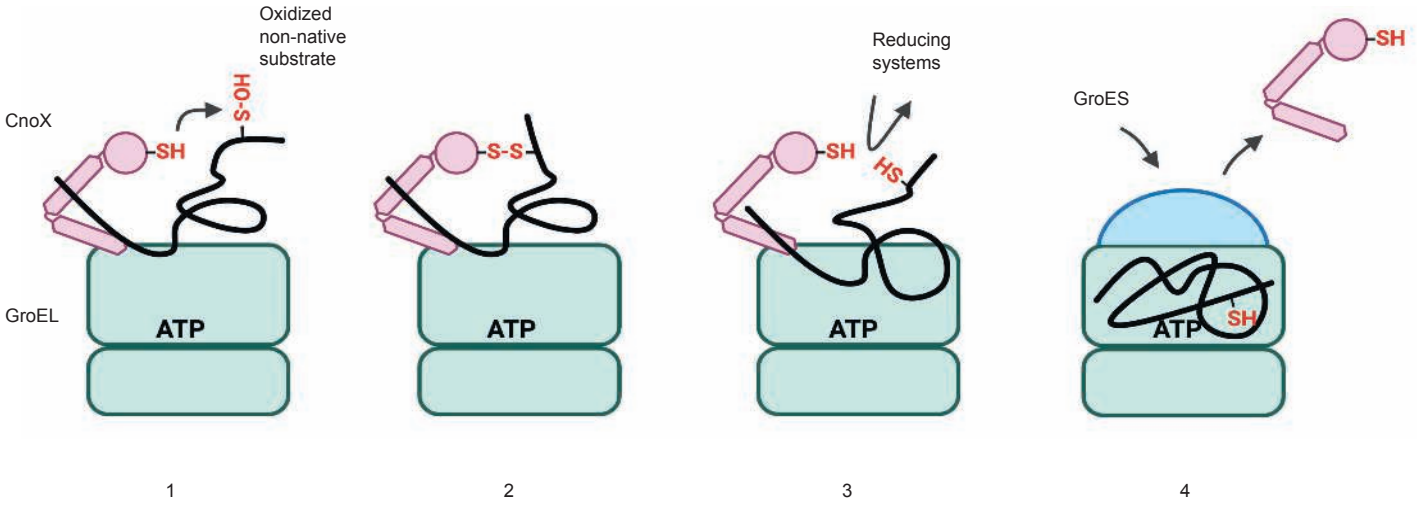

Figure 5

A

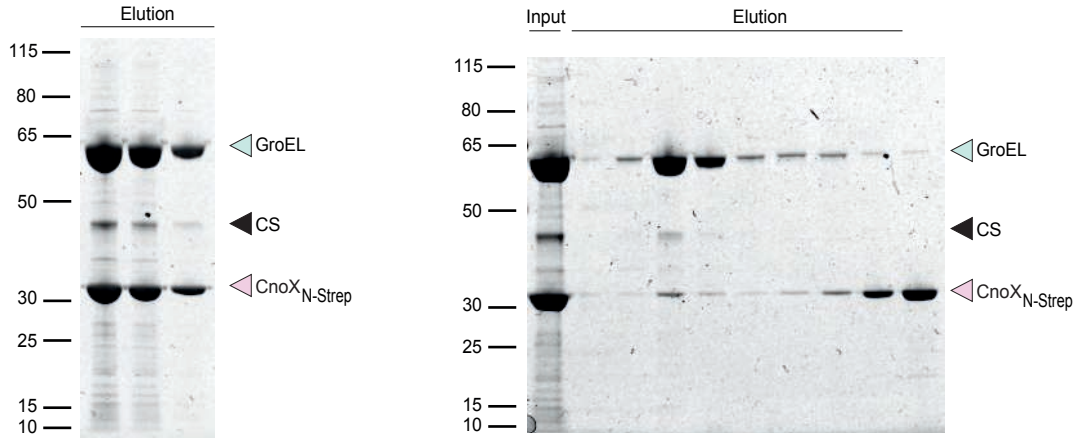

B

CS peptides crosslinked to GroEL peptides

$_{275}$MLEEISSV[K]HIPEFVR$_{290}$	$_{37}$NVVLD[K]SFGAPTITK$_{51}$
$_{308}$VY[K]NYDPR$_{315}$	$_{37}$NVVLD[K]SFGAPTITK$_{51}$
$_{423}$SDI[K]R$_{427}$	$_{119}$GID[K]AVTAAVEELK$_{132}$
$_{411}$QLYTGYE[K]R$_{419}$	$_{119}$GID[K]AVTAAVEELK$_{132}$
$_{308}$VY[K]NYDPR$_{315}$	$_{323}$VVIN[K]DTTTIIDGVGEEAAIQGR$_{345}$
$_{308}$VY[K]NYDPR$_{315}$	$_{383}$VGAATEVEM[K]EK$_{392}$
$_{294}$D[K]NDSFR$_{300}$	$_{383}$VGAATEVEM[K]EK$_{392}$

C

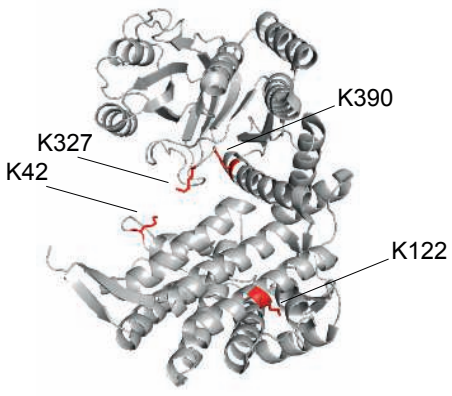

Supplemental Figure S1

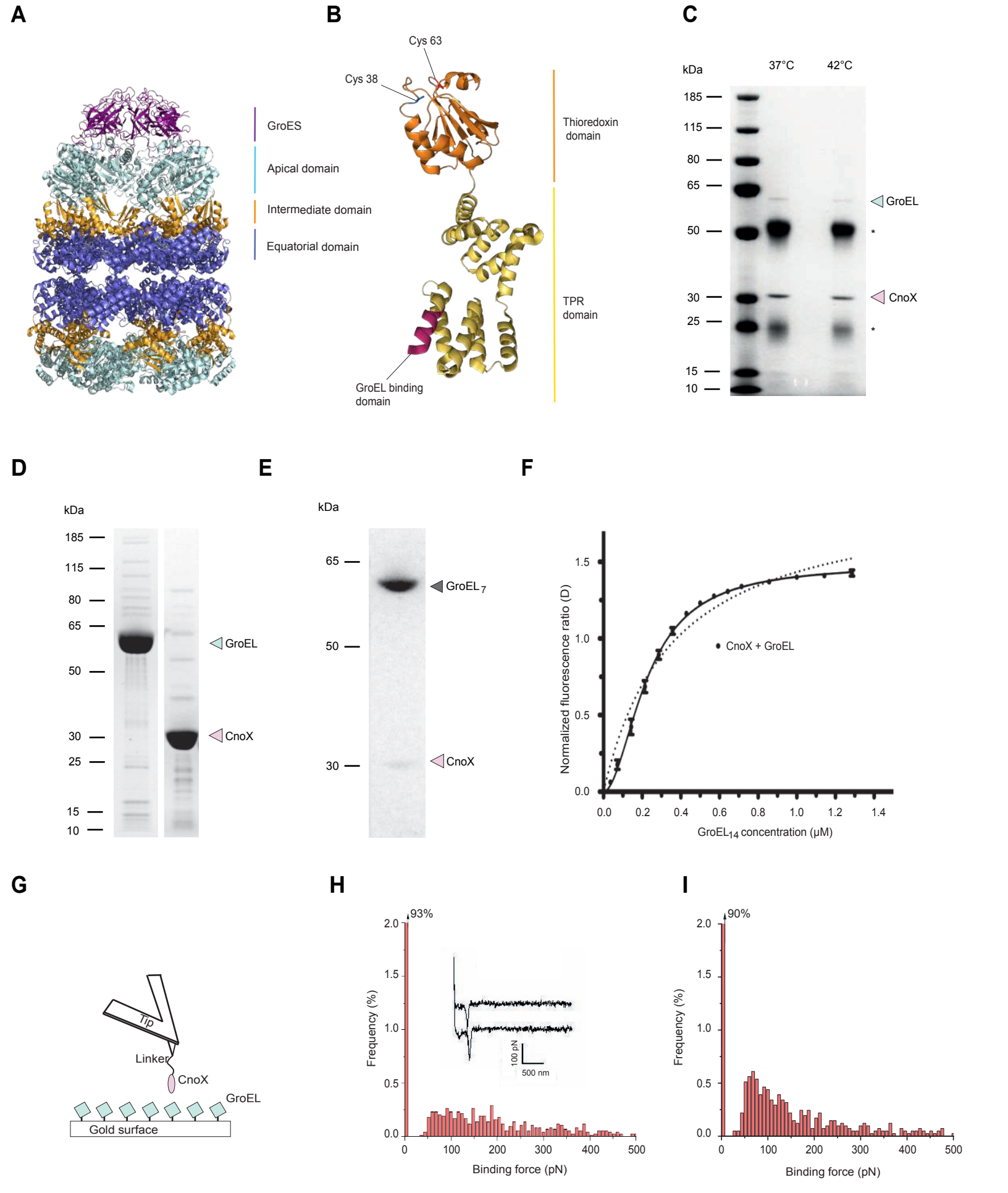

Supplemental Figure S2

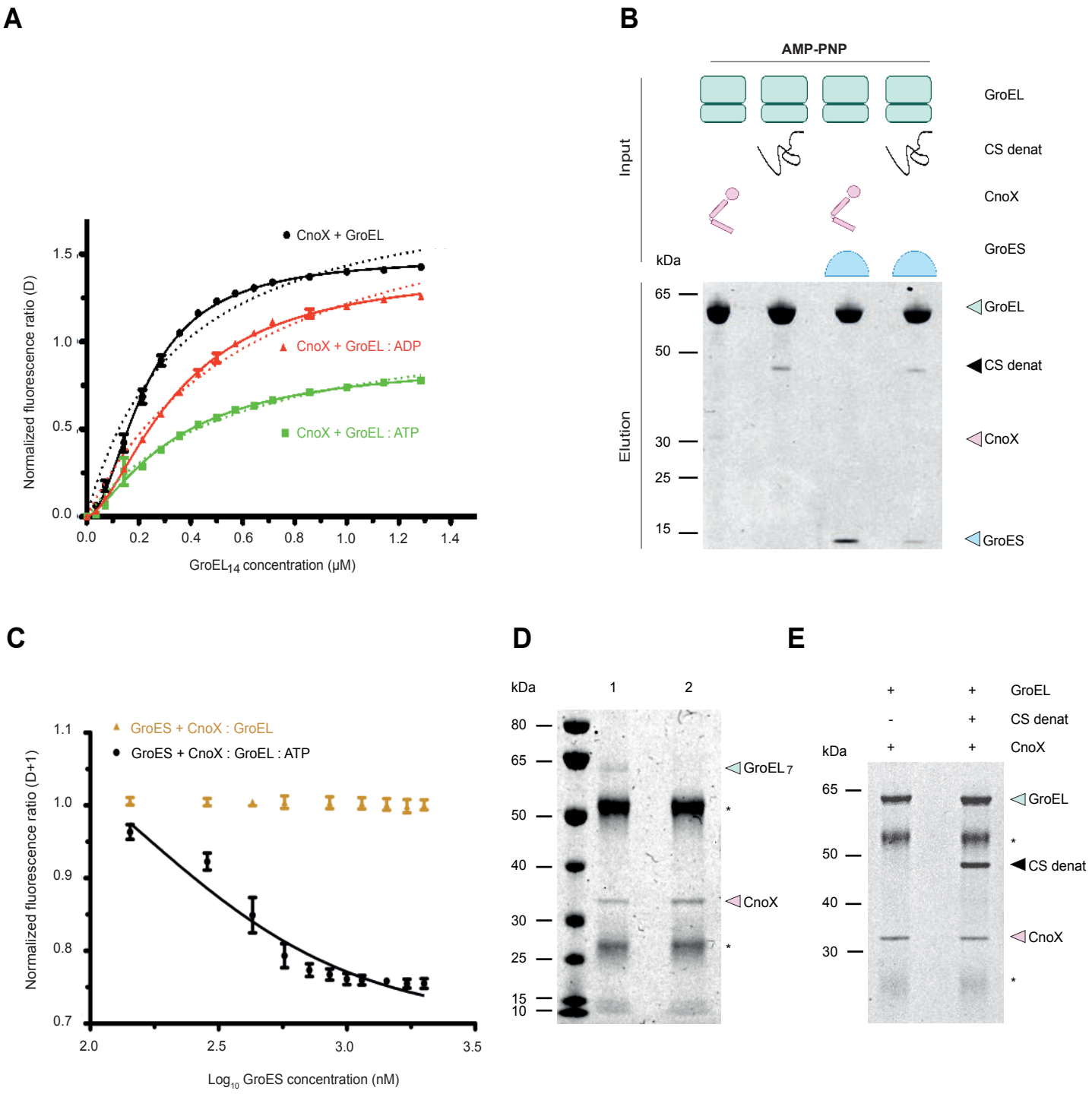

Supplemental Figure S3

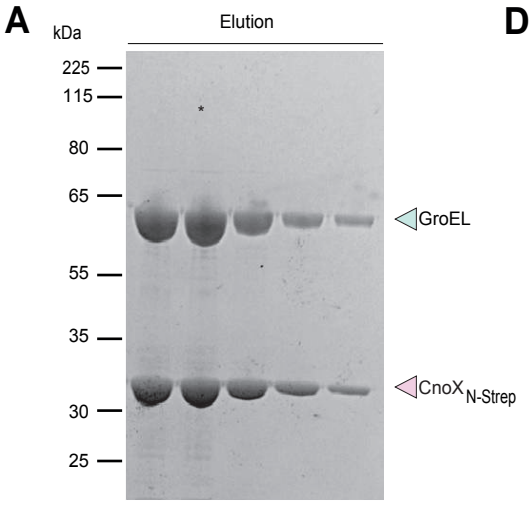

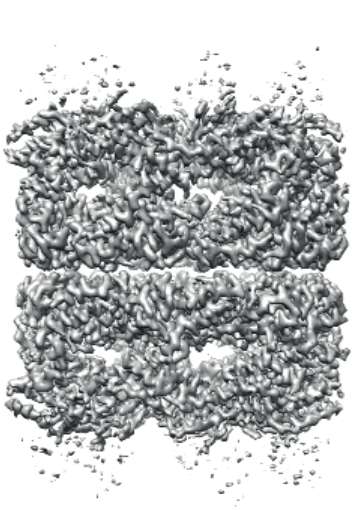

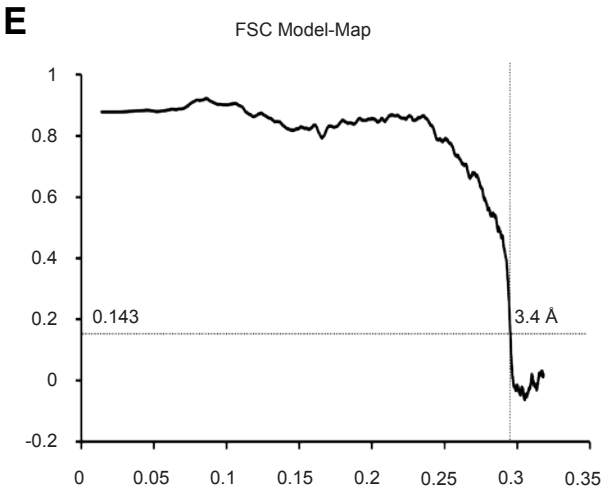

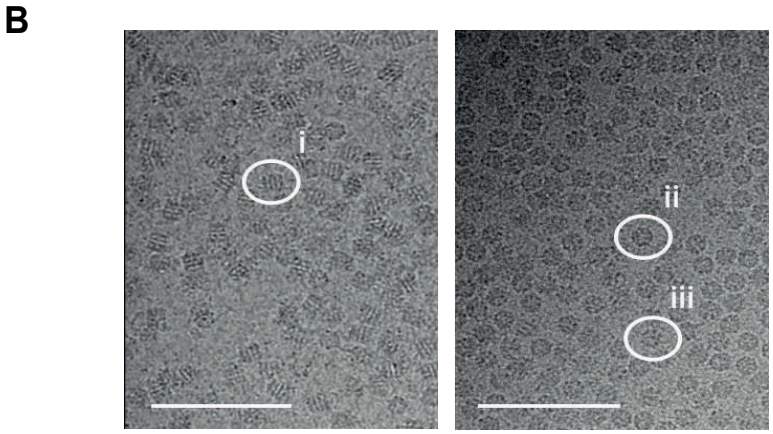

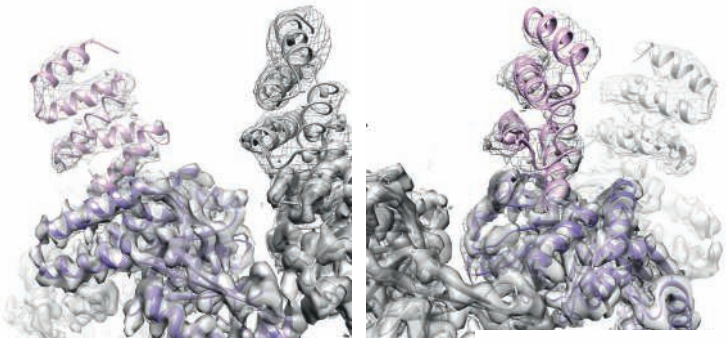

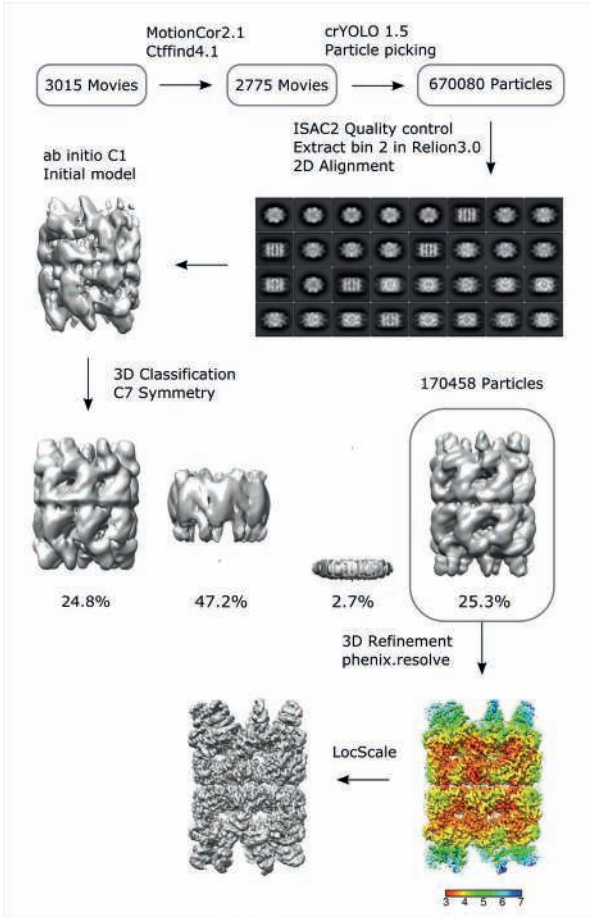

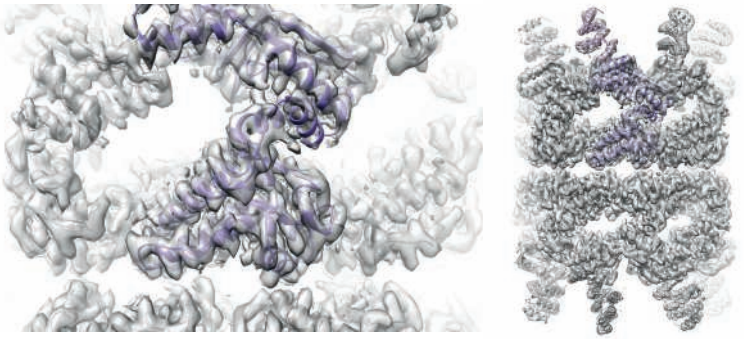

Supplemental Figure S4

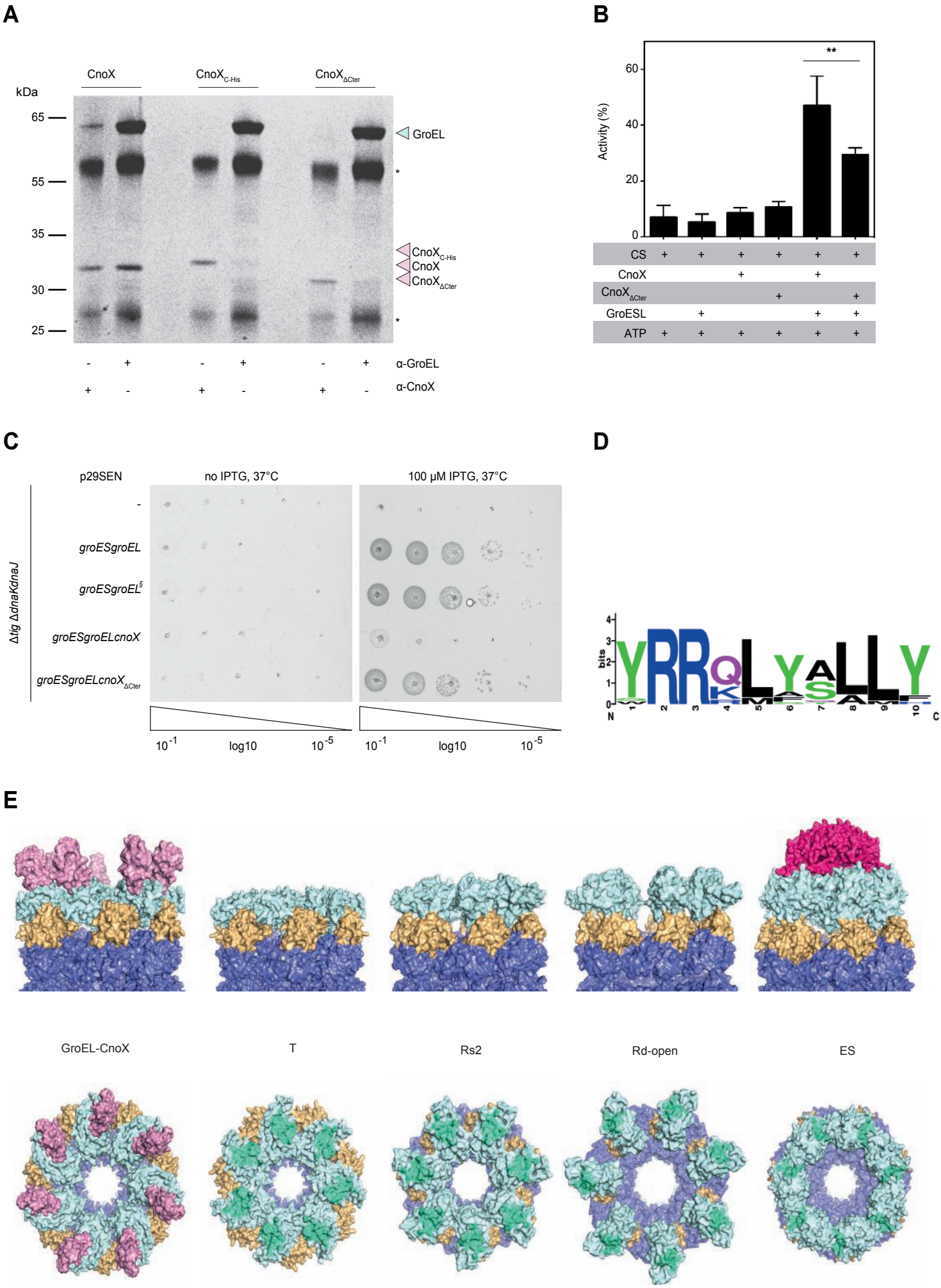

Supplemental Figure S5

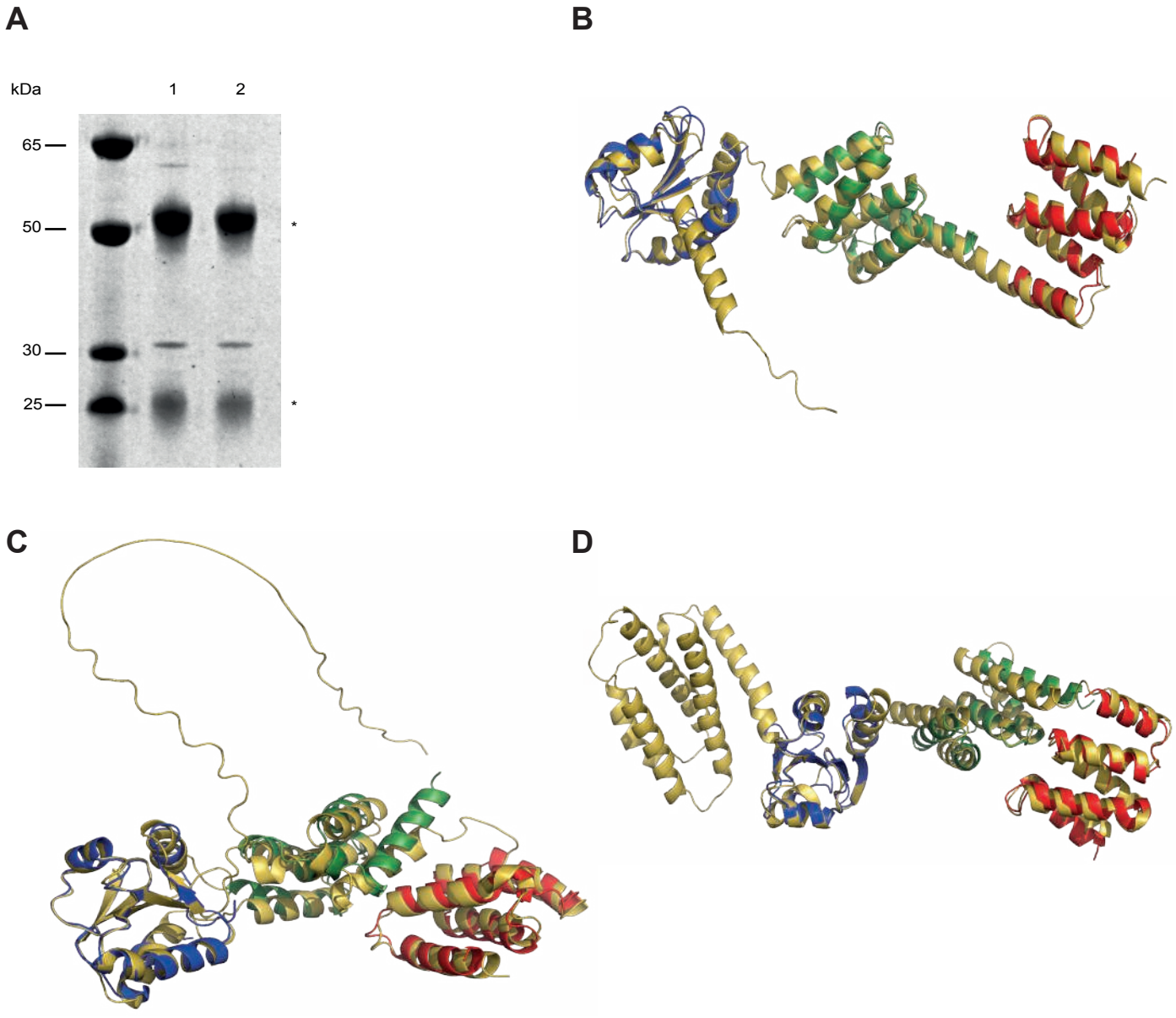

Table S1: CryoEM statistics, related to Figure 2.

	GroEL:CnoX (EMDB-14352) (PDB 7YWY)
Data collection and processing	JEOL CryoARM300, BECM, Brussels
Magnification	60.000
Voltage (kV)	300
Electron exposure (e–/Å2)	68.3
Defocus range (μm)	-0.5 to -3
Pixel size (Å)	0.784
Symmetry imposed	C7
Initial particle images (no.)	670080
Final particle images (no.)	170458
Map resolution (Å)	3.4
FSC threshold	0.143
Map resolution range (Å)	3.1–7.6
Refinement	
Initial model used (PDB code)	1XCK (GroEL), 3QOU (CnoX)
Model resolution (Å)	3.4
FSC threshold	0.143
Map sharpening *B* factor ($Å^2$)	Local sharpening-density modification
Model composition	
Non-hydrogen atoms	63994
Protein residues	8568
Ligands	0
***B* factor ($Å^2$)**	
Proteins	120.42
Ligands	0
RMS deviations	
Bond length (Å)	0.010
Bond angle (°)	1.249
Validation	
MolProbity score	2.04
Clashscore	7.91
Poor rotamers (%)	2.10
Ramachandran plot	
Favored (%)	94.75
Allowed (%)	4.76
Disallowed (%)	0.49

EMDB: Electron Microscopy Data Bank; FSC: Fourier shell correlation; RMS: root mean square.

Table S3: Bacterial strains used in this study, related to STAR Methods.

Strain	Genotype	Plasmid	Source and notes
JF179	MG1655 *wt*		From Jim Bardwell (University of Michigan)
ED002	MG1655 *ΔcnoX*		Goemans et al., 2018
ED004	MG1655 *ΔcnoX*	pET22b-cnoX	Goemans et al., 2018
ED207	MG1655 *ΔcnoX*	pET22b-cnoX$_{R277L}$	This study
ED217	MG1655 *ΔcnoX*	pET22b-cnoX$_{Y284L}$	This study
ED006	MG1655 *ΔcnoX*	pET22b-cnoX$_{C\text{-}His}$	This study
ED005	MG1655 *ΔcnoX*	pET22b-cnoX$_{\Delta Cter}$	This study
CG233	BL21 (DE3)	pET22b-groL	Goemans et al., 2018
ED035	BL21 (DE3)	pET22b-groL$_{D490C}$	This study
ED126	BL21 (DE3)	pET22b-groL$_{R452A/E461A/S463A/V464A}$	This study; Weissman et al., 1995, 1996
ED187	BL21 (DE3)	pET22b-groL$_{G298A/T299L/V300K/E304L/I305K/M307K/R345L}$	This study
CG183	BL21 (DE3)	pET22b-groS	This study
CG232	BL21 (DE3)	pET22b-cnoX	Goemans et al., 2018
CG229	BL21 (DE3)	pET22b-cnoX$_{\Delta Cter}$	This study
CG191	BL21 (DE3)	pET22b-cnoX$_{C\text{-}His}$	This study
CG260	BL21 (DE3)	pET22b-cnoX$_{C38A/C63A}$	Goemans et al., 2018
ED042	BL21 (DE3)	pET22b-cnoX$_{N\text{-}link/C38A/C63A}$	This study
ED145	BL21 (DE3)	pET22b-mhsp60	This study
ED049	BL21 (DE3)	pACYCDuet-1-cnoX$_{N\text{-}Strep}$	This study

Table S4: Plasmids used in this study, related to STAR Methods.

Plasmid	Vector	Protein encoded	Source and notes
pET22b(+)	IPTG-inducible P_{lac}, ampicillin		Novagen
pET22b-cno*X*	pET22b(+)	CnoX	Goemans et al., 2018
pET22b-groL	pET22b(+)	GroEL	Goemans et al., 2018
pET22b-groL$_{D490C}$	pET22b(+)	GroEL$_{D490C}$	This study
pET22b-groL$_{R452A/E461A/S463A/V464A}$	pET22b(+)	GroEL$_{R452A/E461A/S463A/V464A}$	This study; Weissman et al., 1995, 1996
pET22b-groL$_{G298A/T299L/V300K/E304L/I305K/M307K/R345L}$	pET22b(+)	GroEL$_{G298A/T299L/V300K/E304L/I305K/M307K/R345L}$	This study
pET22b-groS	pET22b(+)	GroES	This study
pET22b-cnoX$_{\Delta Cter}$	pET22b(+)	CnoX without the last 10 C-terminal amino acids	This study
pET22b-cnoX$_{C\text{-}His}$	pET22b(+)	CnoX fused with a C-terminal 6xHis tag	This study
pET22b-cnoX$_{C38A/C63A}$	pET22b(+)	CnoX$_{C38A/C63A}$	Goemans et al., 2018
pET22b-cnoX$_{N\text{-}link/C38A/C63A}$	pET22b(+)	CnoX$_{C38A/C63A}$ with an N-terminal cysteine linker (M/A/C/A/G residues)	This study
pACYCDuet-1	IPTG-inducible P_{lac}, chloramphenicol		Novagen
pACYCDuet-1-cnoX$_{N\text{-}Strep}$	pACYCDuet-1	CnoX fused with an N-terminal Strep-tag	This study
MAC-C-CH60	MAC-tag-C	CH60 from *H. sapiens* (HSPD1)	Addgene
pET22b-mhsp60	pET22b(+)	CH60 with the MTS substituted by M/G/S residues	This study
pET15b-cnoX	pET15b	CnoX with thrombin-cleavable N-terminal 6xHis tag	Lin & Wilson, 2011
pET15b-groS	pET15b	GroES with thrombin-cleavable N-terminal 6xHis tag	Lin & Wilson, 2011
pET15b-groL	pET15b	Native GroEL with no tag	This study

IPTG: isopropyl β-D-1-thiogalactopyranoside, MTS: mitochondrial targeting sequence.

Table S5: Primers used in this study, related to STAR Methods.

Primer	Sequence (5' -> 3')	Comments
AGo230_cnoX_Strep_NcoI_F	AAAACCATGGCAAGCTGGAGCCACCCGCAGTTCGAAAAGTCCGTAGAAAATATTGTCAAC	cloning (pACYCDuet-1-cnoX$_{N\text{-}Strep}$)
AGo231_cnoX_Strep_BamHI_R	AAAAGGATCCTCAATACAACAATGCATACAGC	cloning (pACYCDuet-1-cnoX$_{NterStrep}$)
CGo174_GroES_NdeI_F	GAGCATATGAAGTTTCGTCCC	cloning (pET22b-groS)
CGo185_GroES_stop_XhoI_R	GAGCTCGAGTTAGGCTTCGACCACGCC	cloning (pET22b-groS)
CGo178_cnoX_H6_NdeI_F	GAGCATATG*CACCACCACCACCACCAC*TCCCTGATCGGC	cloning (pET22b-cnoX$_{C\text{-}His}$)
CGo71_cnoX_H6-stop_XhoI_R	CTCCTCGAGTCAGTGGTGGTGGTGGTGGTGGCTGAAGAGGATCGAGG	cloning (pET22b-cnoX$_{C\text{-}His}$)
CGo57_cnoX_NdeI_F	GAGCATATGATGTCCCTGATCGGC	cloning (pET22b-cnoX$_{\Delta Cter}$)
CGo234_cnoXdel10_HindIII_stop_R	CTCAAGCTTTCACTTCGACGCCAGTGCATCACC	cloning (pET22b-cnoX$_{\Delta Cter}$)
EDo227_22b(mHSP60)_F	TGAGATCCGGCTGCTAAC	cloning (pET22b-mhsp60)
EDo228_22b(mHSP60)_R	ATGTATATCTCCTTCTTAAAGTTAAACAAAATTATTTC	cloning (pET22b-mhsp60)
EDo229_(22b)mHSP60_F	TTTAAGAAGGAGATATACATATGGGAAGTGCCAAAGATGTAAAATTTGGTGC	cloning (pET22b-mhsp60)
EDo230_(22b)mHSP60_R	TTGTTAGCAGCCGGATCTCAGAACATGCCACCTCCCATAC	cloning (pET22b-mhsp60)
EDo31_GroEL-D490C_F	TGGATCCAGGATACCCATGCAGATCATGTTGCCGTATTCT	cloning (pET22b-groEL$_{D490C}$)
EDo32_GroEL-D490C_R	AGAATACGGCAACATGATCTGCATGGGTATCCTGGATCCA	cloning (pET22b-groEL$_{D490C}$)
EDo321_AD_groEL_G298A-T299L-E304L-R345L_Gibson_frag1_F	GACTGGCGCGCTTGTGATCTCTGAACTTATCG	cloning (pET22b-groL$_{G298A/T299L/V300K/E304L/I305K/M307K/R345L}$)
EDo322_AD_groEL_G298A-T299L-E304L-R345L_Gibson_frag1_R	GTCACGCTCGTCGTTTGGTATGGCTTCATTC	cloning (pET22b-groL$_{G298A/T299L/V300K/E304L/I305K/M307K/R345L}$)
EDo323_AD_groEL_G298A-T299L-E304L-R345L_Gibson_frag2_F	TACCAAACGACGAGCGTGACACCACGATG	cloning (pET22b-groL$_{G298A/T299L/V300K/E304L/I305K/M307K/R345L}$)

EDo324_AD_groEL_G298A-T299L-E304L-R345L_Gibson_frag2_R	AGATCACAAGCGCGCCAGTCAGGGTTGCGATATC	cloning (pET22b-groL$_{G298A/T299L/V300K/E304L/I305K/M307K/R345L}$)
EDo325_AD_groEL_G298A-T299L-V300K-E304L-I305K-M307K-R345L_Gibson_frag1_F	AATCCAGGGCCTTGTTGCTCAGATCCGTCAGCAG	cloning (pET22b-groL$_{G298A/T299L/V300K/E304L/I305K/M307K/R345L}$)
EDo326_AD_groEL_G298A-T299L-V300K-E304L-I305K-M307K-R345L_Gibson_frag1_R	CTTTACCTTTAAGTTCAGAGATTTTAAGCGCGCCAGTCAGGGT	cloning (pET22b-groL$_{G298A/T299L/V300K/E304L/I305K/M307K/R345L}$)
EDo327_AD_groEL_G298A-T299L-V300K-E304L-I305K-M307K-R345L_Gibson_frag2_F	AAAATCTCTGAACTTAAAGGTAAAGAGCTGGAAAAAGC	cloning (pET22b-groL$_{G298A/T299L/V300K/E304L/I305K/M307K/R345L}$)
EDo328_AD_groEL_G298A-T299L-V300K-E304L-I305K-M307K-R345L_Gibson_frag2_R	GAGCAACAAGGCCCTGGATTGCAGCTTC	cloning (pET22b-groL$_{G298A/T299L/V300K/E304L/I305K/M307K/R345L}$)
EDo34_22b_MACAG_cnoX_F	ATGGCTTGTGCTGGTATGTCCGTAGAA	cloning (pET22b- cnoX$_{N\text{-}link/C38A/C63A}$)
EDo35_22b_MACAG_cnoX_R	ACCAGCACAAGCCATCATATGTATAATC	cloning (pET22b-cnoX$_{N\text{-}link/C38A/C63A}$)
EDo92_22b_groEL_R452A_F	AGCTCCGCTGGCTCAGATCGTATTGAACTGC	cloning (pET22b-groL$_{R452A/E461A/S463A/V464A}$)
EDo93_22b_groEL_R452A_R	TCCATTGCACGCAGTGCA	cloning (pET22b-groL$_{R452A/E461A/S463A/V464A}$)
EDo94_22b_groEl_E461A/S463A/V464A_F	GCTGCTGTTGCTAACACCGTTAAAG	cloning (pET22b-groL$_{R452A/E461A/S463A/V464A}$)
EDo95_22b_groEl_E461A/S463A/V464A_R	CGGAGCTTCGCCGCAGTTCAATAC	cloning (pET22b_groL$_{R452A/E461A/S463A/V464A}$)
CnoX_NdeI_for	GCCGACGCCCCTTGCATATGTCCGTAGAAAATATTGTC	cloning (pET15b-cnoX)
CnoX_XhoI_rev	CCGTGCTTTCTTGCTCGAGTCAATACAACAATGCATACAGC	cloning (pET15b-cnoX)
GroES_NdeI_for	CCTGAGAAGCGTTCCATATGAATATTCGTCCATTGCATGATCG	cloning (pET15b -groS)
GroES_XhoI_rev	CCGTGCTGCCTTGCTCGAGTTACGCTTCAACAATTGCCAGAATG	cloning (pET15b -groS)
GroEL_mHis_for	CTTTAAGAAGGAGATATACCCATATGGCAGCTAAAGACGTAAAATTC	cloning (pET15b-groL)
GroEL_mHis_rev	GAATTTTACGTCTTTAGCTGCCATATGGGTATATCTCCTTCTTAAAG	cloning (pET15b-groL)